15. Fithian DC, Paxton EW, Stone ML, Luetzow WF, Csintalan RP et al (2005) Prospective trial of a treatment algorithm for the management of the anterior cruciate ligament–injured knee. Am J Sports Med 33:335–346
16. Harter RA, Osternig LR, Singer KM, James SL, Larson RL et al (1988) Long-term evaluation of knee stability and function following surgical reconstruction for anterior cruciate ligament insufficiency. Am J Sports Med 16:434–443
17. Herrington L, Wrapson C, Matthews M, Matthews H (2005) Anterior cruciate ligament reconstruction, hamstring versus bone-patella tendon-bone grafts: a systematic literature review of outcome from surgery. Knee 12:41–50
18. Hertel P, Behrend H, Cierpinski T, Musahl V, Widjaja (2005) ACL reconstruction using bone-patellar tendon-bone press-fit fixation: 10-year clinical results. Knee Surg Sports Traumatol Arthrosc 13:248–255
19. Howell SM, Clark JA (1992) Tibial tunnel placement in anterior cruciate ligament reconstructions and graft impingement. Clin Orthop Relat Res 283:187–95
20. Johnston DR, Baker A, Rose C, Scotland TR, Maffulli N (2003) Long-term outcome of MacIntosh reconstruction of chronic anterior cruciate ligament insufficiency using fascia lata. J Orthop Sci 8:789–795
21. Jomha NM, Borton DC, Clingeleffer AJ, Pinczewski LA (1999) Long-term osteoarthritic changes in anterior cruciate ligament reconstructed knees. Clin Orthop Relat Res 358:188–193
22. Jomha NM, Pinczewski LA, Clingeleffer A, Otto DD (1999) Arthroscopic reconstruction of the anterior cruciate ligament with patellar-tendon autograft and interference screw fixation. The results at seven years. J Bone Joint Surg Br 81:775–779
23. Jorgensen U, Bak K, Ekstrand J, Scavenius M (2001) Reconstruction of the anterior cruciate ligament with the iliotibial band autograft in patients with chronic knee instability. Knee Surg Sports Traumatol Arthrosc 9:137–145
24. Kullmer K, Letsch R, Turowski B (1994) Which factors influence the progression of degenerative osteoarthritis after ACL surgery? Knee Surg Sports Traumatol Arthrosc 2:80–84
25. Meystre JL, Vallotton J, Benvenuti JF (1998) Double semitendinosus anterior cruciate ligament reconstruction: 10-year results. Knee Surg Sports Traumatol Arthrosc 6:76–81
26. Murray AW, Macnicol MF (2004) 10–16 year results of Leeds-Keio anterior cruciate ligament reconstruction. Knee 11:9–14
27. Noyes FR, Barber-Westin SD (1996) Reconstruction of the anterior cruciate ligament with human allograft. Comparison of early and later results. J Bone Joint Surg Am 78:524–537
28. Ruiz AL, Kelly M, Nutton RW (2002) Arthroscopic ACL reconstruction: a 5–9 year follow-up. Knee 9:197–200
29. Sernert N, Kartus J, Kohler K, Stener S, Larsson J et al (1999) Analysis of subjective, objective and functional examination tests after anterior cruciate ligament reconstruction. A follow-up of 527 patients. Knee Surg Sports Traumatol Arthrosc 7:160–165
30. Shelbourne KD, Gray T (2000) Results of anterior cruciate ligament reconstruction based on meniscus and articular cartilage status at the time of surgery. Five- to fifteen-year evaluations. Am J Sports Med 28:446–452
31. Sherman OH, Banffy MB (2004) Anterior cruciate ligament reconstruction: which graft is best? Arthroscopy 20:974–980
32. Tegner Y, Lysholm J (1985) Rating systems in the evaluation of knee ligament injuries. Clin Orthop Relat Res 198:43–49
33. Terry GC, Hughston JC, Norwood LA (1986) The anatomy of the iliopatellar band and iliotibial tract. Am J Sports Med 14:39–45
34. Yunes M, Richmond JC, Engels EA, Pinczewski LA (2001) Patellar versus hamstring tendons in anterior cruciate ligament reconstruction: a meta-analysis. Arthroscopy 17:248–257

Precise Control of Lower Critical Solution Temperature of Thermosensitive Poly(2-isopropyl-2-oxazoline) via Gradient Copolymerization with 2-Ethyl-2-oxazoline as a Hydrophilic Comonomer

Joon-Sik Park[†] and Kazunori Kataoka*[,†,‡,§]

Department of Materials Engineering, Graduate School of Engineering, The University of Tokyo, 7-3-1 Hongo, Bunkyo-ku, Tokyo 113-8656, Japan; Center for Disease Biology and Integrative Medicine, Graduate School of Medicine, The University of Tokyo, Tokyo 113-0033, Japan; and Center for NanoBio Integration, The University of Tokyo, 7-3-1 Hongo, Bunkyo-ku, Tokyo 113-8656, Japan

Received March 13, 2006; Revised Manuscript Received June 23, 2006

ABSTRACT: The lower critical solution temperature (LCST) of amphiphilic poly(2-isopropyl-2-oxazoline) (P*i*PrOx) was precisely tuned via the copolymerization with 2-ethyl-2-oxazoline (EtOx) as a hydrophilic comonomer. The copolymerization was cationically initiated by methyl *p*-tosylate at the optimum condition (42 °C in acetonitrile) for living polymerization, obtaining the copolymers with a narrow molecular weight distribution ($M_w/M_n \leq 1.02$). The monomer reactivity ratios of 1.78 and 0.79 respectively were derived for EtOx and *i*PrOx from the cumulative and instantaneous compositions of the copolymers determined from the ^{1}H NMR and MALDI-TOF mass spectrometry. This set of the reactivity ratios are sufficiently different enough to form the gradient copolymers, in which each polymer chain has a trend of a gradually decreasing EtOx and an increasing *i*PrOx composition along the backbone from the α-terminal to ω-chain end. These gradient copolymers followed a rather simple rule in their thermosensitive behaviors to show a linear increase in LCST with an increasing mol % of EtOx. Consequently, a series of P(EtOx-*co*-*i*PrOx) with finely tuned LCST in aqueous medium were obtained through the cationic copolymerization simply by varying the initial composition of both monomers, opening a new way to engineer the thermosensitivity of polymeric materials directing to particular applications.

Introduction

Recently, enormous attention has been paid to so-called "smart" polymeric materials showing a discrete change in their propensity responding to external physical and chemical stimuli, including light, temperature, pH, and magnetic and electric fields. Of special interest is temperature-responsive polymers useful for various practical applications, such as supports for catalysts,[1] sensors,[2] separation systems,[3] enzymatic bioconjugates,[4] and drug carriers.[5] Drastic changes in solubility, turbidity, and other physicochemical properties of thermosensitive polymers can be simply induced by adding or removing heat energy, and such feasibility is particularly important to design "smart" polymeric materials that instantly respond to the external stimuli. Careful engineering of polymer structure should be needed for the fine-tuning of responding temperature as well as sharpness of transition. Furthermore, additional functionalization in a controllable manner may be required for some applications directing to construct thermosensitive block or graft copolymers, which have received growing interest particularly in bio-related fields.

In this regard, we have been recently focusing on the quantitative polymerization and selective end-functionalization of thermosensitive poly(2-isopropyl-2-oxazoline) (P*i*PrOx) telechelics.[6] The polymerization proceeded in a good controlled manner under an optimum temperature condition (42 °C) with appreciably narrow molecular weight distributions ($M_w/M_n \leq$ 1.03), having never been accomplished in those of the conventional poly(2-oxazolines) (POx) homologues often viewed as "pseudopeptides".[7] Of importance is that P*i*PrOx exhibits a characteristic lower critical solution temperature (LCST) near physiological conditions, like poly(*N*-isopropylacrylamide) (PNIPAAm),[8] the typical representative of the thermosensitive polymers with numerous applications. The notable transition behaviors of P*i*PrOx, characterized by a fast responsivity, viz., transition sharpness, could be achieved by the precise control of the well-defined polymeric structures through the living polymerization mechanism. It should be also noted that POx, as a rule, are nontoxic and that some of them carry US Food and Drug Administration (FDA) approval.[9]

In the meantime, the LCST of P*i*PrOx can be controlled by incorporating the specific composition of hydrophilic or hydrophobic 2-oxazoline monomer units within the main chains, as in the case of conventional thermosensitive polymers.[10] A number of recent studies have shown that thermosensitive copolymers from different monomers are simply synthesized by the living ionic or controlled/living radical polymerization technique, and these copolymers with well-balanced hydrophilic/hydrophobic monomer sequences are attractive to realize the elaborate manipulability of their LCST values.[11] Nevertheless, little attention has been paid to the living cationic copolymerization between 2-isopropyl-2-oxazoline (*i*PrOx) and various hydrophilic/hydrophobic 2-substituted-2-oxazolines (Ox). Although there are several examples of copolymers composed of some Ox sequences including *i*PrOx,[12] the study on the LCST control of POx through the well-defined cationic copolymerization of *i*PrOx with either the hydrophilic or hydrophobic Ox comonomer has not been accomplished yet. Because there are various hydrophilic and hydrophobic Ox monomers, it is

† Graduate School of Engineering.
‡ Graduate School of Medicine.
§ Center for NanoBio Integration.
* To whom correspondence should be addressed: Tel +81-3-5841-7138; Fax +81-3-5841-7139; e-mail kataoka@bmw.t.u-tokyo.ac.jp.

10.1021/ma0605548 CCC: $33.50
Published on Web 08/22/2006

Scheme 1. Synthetic Scheme for the Gradient Copolymerization of 2-Ethyl-2-oxazoline (EtOx) and 2-Isopropyl-2-oxazoline (*i*PrOx) Initiated with Methyl *p*-Tosylate

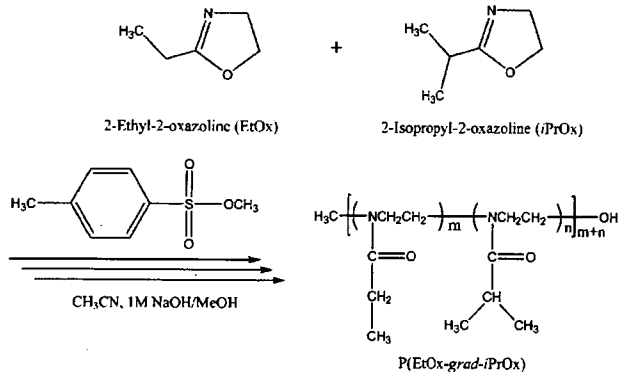

relatively easy to select the appropriate comonomer for varying the solubility of P*i*PrOx in water. However, careful consideration should also be taken into account for the diversity of the copolymerization conditions, derived from the many combinations among initiators, solvents, and temperatures vs the respective Ox monomers. It has been also noted that, in the controlled living copolymerization system of two monomers with sufficiently different reactivity ratios, a gradient copolymer, in which the instantaneous composition continuously varies along the chain contour, could be predominantly produced due to the feed composition drift that spontaneously occurs during the reaction.[13] Therefore, it was hypothesized that the choice of the appropriate hydrophilic or hydrophobic Ox comonomer exhibiting a sufficiently different reactivity against the *i*PrOx monomer may create thermosensitive gradient copolymers.

In the present study, we report the facile and precise synthetic route of thermosensitive gradient copolymers via the living cationic polymerization of *i*PrOx, including the specific composition of EtOx as a hydrophilic comonomer (Scheme 1). It was confirmed from the ^{1}H NMR and MALDI-TOF mass spectrometry that EtOx and *i*PrOx were found to have reactivity ratios sufficiently different from gradient copolymers under mild temperature conditions (42 °C). Furthermore, these POx gradient copolymers showed a rapid and linear response to temperature change from 38.7 to 67.3 °C.

Experimental Section

Materials. 2-Isopropyl-2-oxaxoline was synthesized from isobutyric acid (Wako Pure Chemical Industries, Ltd., Osaka, Japan) and 2-aminoethanol (Wako Pure Chemical Industries) as previously described.[6,14] Methyl *p*-tosylate (Tokyo Kasei Kogyo Co., Ltd., Tokyo, Japan) was distilled from calcium hydride under reduced pressure. 2-Ethyl-2-oxaxoline (Aldrich Chemical Co., Ltd., Milwaukee, WI) and acetonitrile (Wako Pure Chemical Industries) were distilled from calcium hydride following conventional procedures.[15] Other chemicals such as the 1 N NaOH aqueous solution and methanol were purchased from Wako Pure Chemical Industries and used without further purification.

Techniques. The ^{1}H NMR spectra were recorded using a JEOL EX 300 spectrometer at 300 MHz. The chemical shifts were reported in parts per million (ppm) downfield from tetramethylsilane. The molecular weights and molecular weight distributions were determined using a GPC (TOSOH HLC-8220) system equipped with two TSK gel columns (G4000H$_{HR}$ and G3000H$_{HR}$) and an internal refractive index (RI) detector. The columns were eluted with DMF containing lithium bromide (10 mM) and triethylamine (30 mM) at the flow rate of 0.8 mL/min and were maintained at a temperature of 40 °C. The molecular weights were calibrated using poly(ethylene glycol) (PEG) standards (Polymer Laboratories, Ltd., UK). The mass measurements were performed using a MALDI-TOF mass spectrometer (Bruker REFLEX III), operating at an acceleration voltage of 23 kV in the reflection mode. The UV−vis spectra were obtained using a V-550 UV/vis JASCO spectrophotometer.

Synthesis of Poly(2-isopropyl-2-oxazoline) (P*i*PrOx) Having a Hydroxyl Group at the ω-Terminal End. 2-Isopropyl-2-oxazoline (*i*PrOx) (10 g, 88.4 mmol) was added via a syringe to a solution of methyl *p*-tosylate (MeOTs) (0.186 g, 1.0 mmol) in acetonitrile (30 mL). The polymerization mixture was stirred at 42 °C for 476.5 h under an argon atmosphere. The mixture was cooled to room temperature and treated with methanolic NaOH (1 M) to introduce a hydroxyl group at one of the chain ends. The solution of Me-P*i*PrOx-OH was purified via dialysis for 2 days against distilled water and then recovered by lyophilization. Six samples were collected during the course of the polymerization. They were subjected to the same treatment above and analyzed by a MALDI-TOF mass spectrometer in order to determine the conversion yield (total yields: 9 g, 90%).

Synthesis of Poly(2-ethyl-2-oxazoline) (PEtOx) Having a Hydroxyl Group at the ω-Terminal End. 2-Ethyl-2-oxazoline (EtOx) (8.763 g, 88.4 mmol) was added via a syringe to a solution of MeOTs (0.186 g, 1.0 mmol) in acetonitrile (30 mL). The polymerization mixture was stirred at 42 °C for 315 h under an argon atmosphere. The mixture was then cooled to room temperature and treated with methanolic NaOH (1 M) to introduce a hydroxyl group at one of the chain ends. The solution of Me-PEtOx-OH was purified via dialysis for 2 days against distilled water and then recovered by lyophilization. Four samples were collected during the course of the polymerization. They were subjected to the same treatment described above and analyzed using a MALDI-TOF mass spectrometer in order to determine the conversion yield (total yields: 8.3 g, 95%).

Synthesis of Gradient Copolymers (P(EtOx$_{25\%}$*i*PrOx$_{75\%}$), P(EtOx$_{50\%}$*i*PrOx$_{50\%}$), P(EtOx$_{75\%}$*i*PrOx$_{25\%}$)) Having a Hydroxyl Group at the ω-Terminal End. The respective mixtures of 2-ethyl-2-oxazoline (EtOx$_{25\%}$: 2.19 g, 22.1 mmol; EtOx$_{50\%}$: 4.38 g, 44.2 mmol; EtOx$_{75\%}$: 6.57 g, 66.3 mmol) and 2-isopropyl-2-oxazoline (*i*PrOx$_{75\%}$: 7.5 g, 66.3 mmol; *i*PrOx$_{50\%}$: 5 g, 44.2 mmol; *i*PrOx$_{25\%}$: 2.5 g, 22.1 mmol) were added to a solution of MeOTs (0.186 g, 1.0 mmol) in acetonitrile (30 mL). The polymerization mixture was stirred at 42 °C for 309.5 h (P(EtOx$_{25\%}$*i*PrOx$_{75\%}$)), 407 h (P(EtOx$_{50\%}$*i*PrOx$_{50\%}$)), and 288 h (P(EtOx$_{75\%}$*i*PrOx$_{25\%}$)) under an argon atmosphere. The reaction mixtures were cooled to room temperature and then treated with methanolic NaOH (1 M) to introduce a hydroxyl group at one of the chain ends. The copolymer solutions were purified via dialysis for 2 days against distilled water and then recovered by lyophilization. Several samples of the respective copolymers were collected during the course of the copolymerization. They were subjected to the same treatment as described above and analyzed by MALDI-TOF mass and ^{1}H NMR spectrometers in order to determine the conversion yield and composition of the copolymers (total yields: 8.4 g, 87% (P(EtOx$_{25\%}$*i*PrOx$_{75\%}$)), 8.5 g, 91% (P(EtOx$_{50\%}$*i*PrOx$_{50\%}$)), 7.7 g, 85% (P(EtOx$_{75\%}$*i*PrOx$_{25\%}$)).

MALDI-TOF Mass Spectrometry. An external calibration was performed using poly(ethylene glycol) standards (MeO-PEG-OH; MW = 5000, 12 000, NOF Corp). Ions were generated by laser desorption at 337 nm (N_2 laser, 3 ns pulse width, 10^6-10^7 W/cm^2). For each spectrum, ~400 transients were accumulated and all spectra were recorded in the reflection mode. The data evaluation was performed with the Bruker XMASS program using the reflection spectra only in order to achieve a better signal-to-noise ratio. α-Cyano-4-hydroxycinnamic acid (CCA) (Fluka) was selected as a suitable matrix. A trifluoroacetic acid/acetonitrile (0.1% TFA: CH_3CN = 2:1) solution of CCA (10 mg/mL) was mixed with a solution of the polymer in acetonitrile (1 mg/mL) at an equimolar ratio. The resulting mixture was shaken for a few seconds. An aliquot of the mixture (1 μL) was placed on the target plate and inserted into the ion source chamber after being slowly dried. The polymer concentration of the polymer/matrix mixture solution could

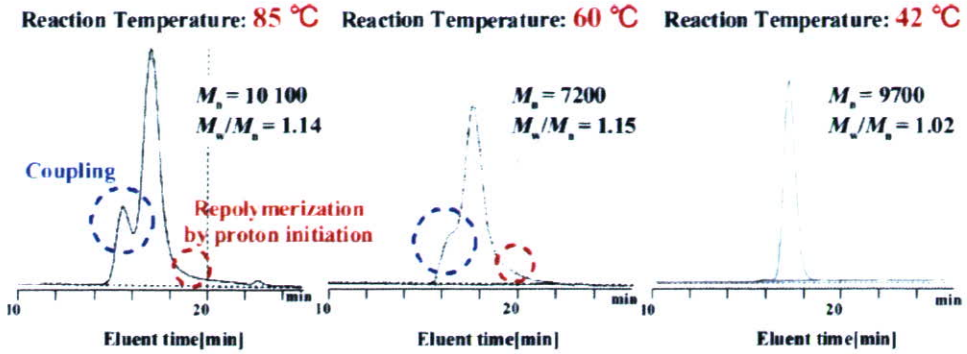

Figure 1. GPC diagrams of P*i*PrOx (DP_{theo} = 88.4) synthesized under different temperature conditions (PEG standard, eluent: DMF (containing 10 mM LiCl and 30 mM TEA), temperature: 40 °C, RI detection).

Table 1. Copolymerization Results of *i*PrOx with EtOx at Different Feed Composition[a] and Their T_{cp} Values

		M_n (M_w/M_n)			
feed ratio (EtOx:*i*PrOx)	yield (%)	MALDI-TOF-MS[b]	GPC[c]	*m*:*n*[d]	T_{cp}[c] (°C) (with 150 mM NaCl)
100:0	95	8300 (1.01)	8000 (1.02)	100:0	
25:75	87	8700 (1.01)	9300 (1.02)	22:78	67.3 (65.4)
50:50	91	9300 (1.01)	9300 (1.02)	48:52	55.2 (54.0)
75:25	85	9100 (1.01)	9300 (1.02)	73:27	46.0 (45.1)
0:100	90	10200 (1.01)	9700 (1.02)	0:100	38.7 (37.4)

[a] Reaction conditions: ([EtOx] + [*i*PrOx])/$[MeOTs]_{init}$ = 88.4, $[MeOTs]_{init}/[CH_3CN]_{solv}$ = 0.033 mol/L, 42 °C, terminated with methanolic NaOH (1 M) for hydroxyl ω-end group. [b] Bruker REFLEX III, operating at an acceleration voltage of 23 kV in the reflector mode. [c] DMF (10 mM LiCl and 30 mM TEA), 40 °C, RI detection. [d] Determined by ^{1}H NMR spectroscopy for the final copolymer products (monomer composition: *m* = [EtOx], *n* = [*i*PrOx]). [e] Measured by UV−vis spectroscopy (*c* = 1.0 wt %).

be diluted for the optimum ionization with an acetone solution of CCA (10 mg/mL).

Turbidity Measurements. Cloud points were determined by spectrophotometric detection of the changes in transmittance (λ = 500 nm) of the aqueous polymer solutions (1.0 wt %) heated at a constant rate (0.5 °C/min). The samples were placed in a temperature-controlled circulating water bath. Values for the cloud points of the polymer solutions were determined as the temperature corresponding to a 10% decrease in optical transmittance.

Results and Discussion

Synthesis of Homopolymers. Prior to the synthesis of copolymers, the respective polymerization behaviors of both the P*i*PrOx and PEtOx homopolymers needed to be screened in order to gain the kinetic information under the identical reaction conditions.

As far as the polymerization of *i*PrOx initiated with methyl *p*-tosylate (MeOTs) in acetonitrile, the mild temperature condition should be adapted for avoiding the spontaneously occurring side reactions such as chain transfer and coupling, resulting in wide molecular weight distributions (Figure 1). There has been an argument that the branching in 2-alkyl-2-oxazoline polymerization is susceptible to occur with the increasing monomer conversion, deriving from a chain transfer to monomer followed by repolymerization and coupling.[16] This effect was visible in the GPC traces of Figure 1 as a lower molecular weight tailing and a higher molecular weight shoulder, even notable with increasing temperature. In particular, at polymerization temperature of 85 °C, the higher molecular weight shoulder on the GPC diagram become pronounced, which is most likely due to the occurrence of a coupling or branching. In the chain transfer step, a monomer, instead of adding nucleophilically to the growing chain end, abstracts a proton to produce a dormant enamine-terminated polymer chain and an oxazolinium monomer which can continue the kinetic chain. In the coupling (or branching) step, after the majority of the presumably more

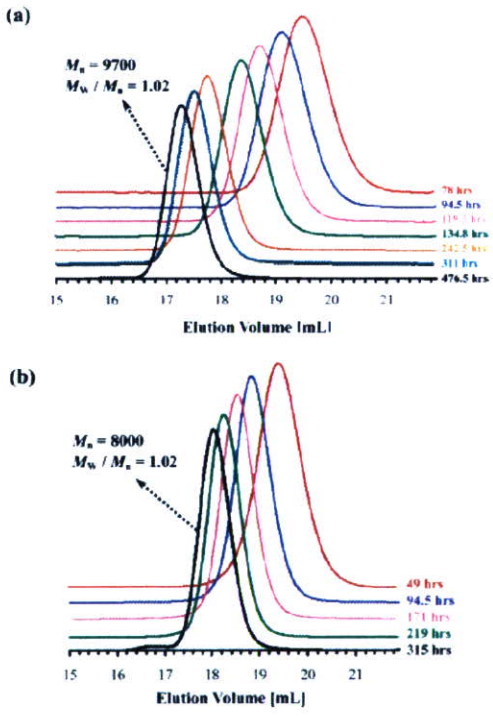

Figure 2. GPC traces of two homopolymers ((a) P*i*PrOx and (b) PEtOx) having different molecular weights (PEG standard, eluent: DMF (containing 10 mM LiCl and 30 mM TEA), temperature: 40 °C, RI detection).

reactive oxazoline monomer is exhausted, the terminal enamine end groups on the dormant chains are able to compete for the oxazolinium chain ends. Each of these couplings produces a branch point and regenerates another oxazolinium end group. The evidence of these side reactions was often observed as both lower molecular weight tailings and higher molecular weight shoulders in the GPC traces of P*i*PrOx, so that the mild

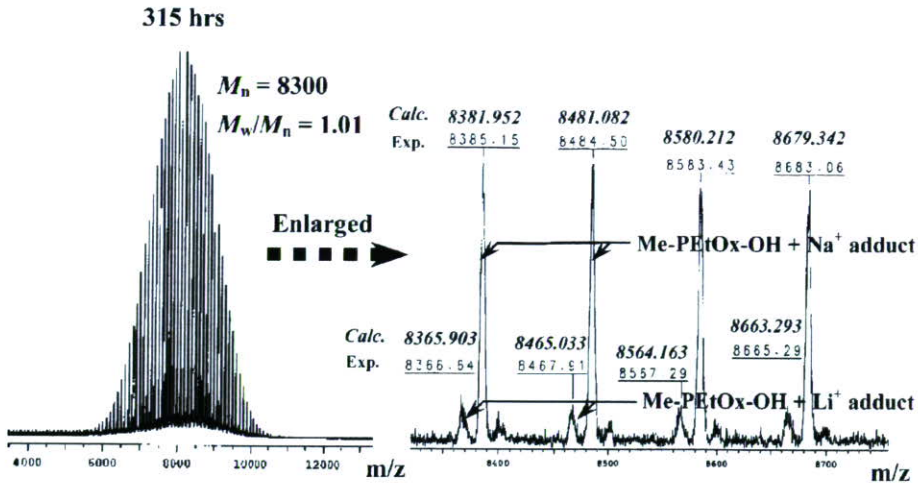

Figure 3. MALDI-TOF mass spectrum of ω-hydroxyl-terminated PEtOx after 315 h (left) and its expanded spectrum in the region of 8330−8750 (right).

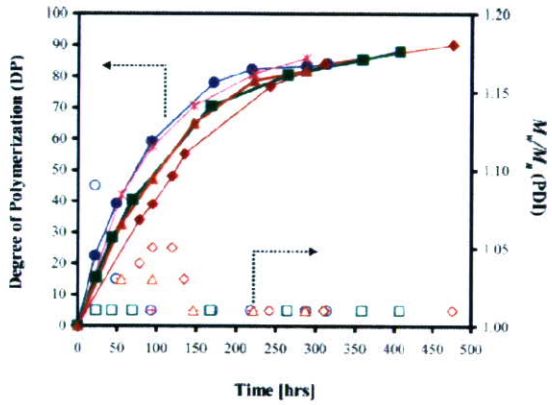

Figure 4. Degree of polymerization (DP) (closed symbols) and polydispersity index (PDI) (open symbols), obtained from MALDI-TOF mass spectrometry, against reaction time for two homopolymers (P*i*PrOx (◆, ◇) and PEtOx (●, ○)) and three gradient copolymers ($P(EtOx_{25\%}iPrOx_{75\%})$ (▲, △), $P(EtOx_{50\%}iPrOx_{50\%})$ (■, □), and $P(EtOx_{75\%}iPrOx_{25\%})$ (*, +)).

temperature of 42 °C was found to be a key condition factor to have complete control over the side reactions (Figure 1).

Based on the results described above, the cationic ring-opening polymerization of *i*PrOx initiated with MeOTs was done to obtain the well-defined poly(2-isopropyl-2-oxazoline) carrying a hydroxyl group at one end (Me-P*i*PrOx-OH). Under mild temperature conditions (42 °C), the polymerization had to be left to proceed for lengths of time up to ca. 476.5 h, but no noticeable side reactions occurred. It was ascertained from the GPC diagrams (Figure 2a) and MALDI-TOF mass spectra (Figure S1a−g in the Supporting Information) that the time-dependent change in the number-average molecular weight (M_n) and the molecular weight distribution were consistent with the living polymerization process; the polydispersity index was low (PDI_{GPC} = 1.02, PDI_{TOF-MS} = 1.01), and the experimental M_n value ($M_{n,GPC}$ = 9700, $M_{n,TOF-MS}$ = 10 200) was close to the value predicted from the initial monomer/initiator ratio ($M_{n,calc}$ = 10 000) (Table 1). An end-group analysis of the polymer was also performed from the MALDI-TOF mass spectrum recorded for a Me-P*i*PrOx-OH after 476.5 h (Figure S1g in the Supporting Information). The most intense signal can be assigned to the sodium adduct of Me-P*i*PrOx-OH, while the second most intense signal is due to the potassium adduct of Me-P*i*PrOx-OH.

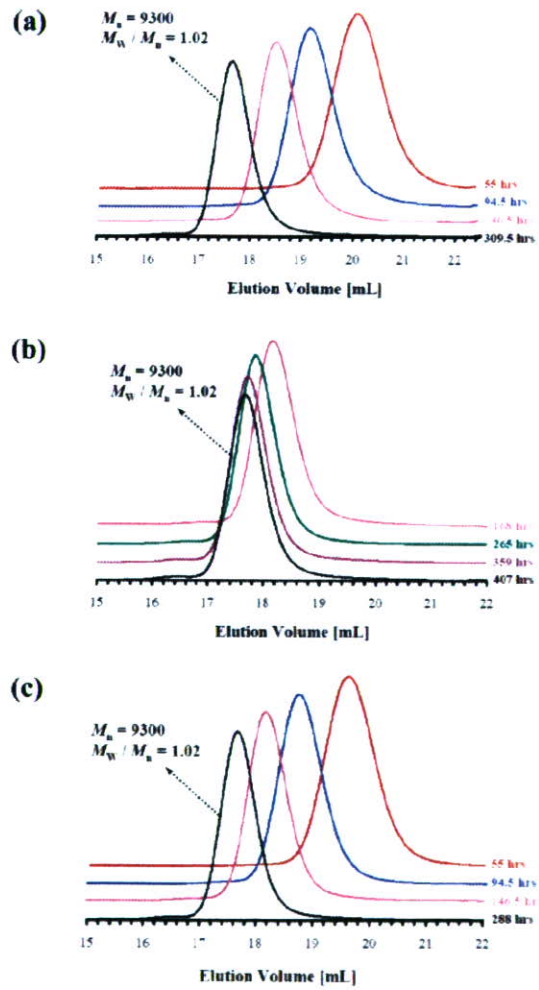

Figure 5. GPC traces of three gradient copolymers ((a) $P(EtOx_{25\%}iPrOx_{75\%})$, (b) $P(EtOx_{50\%}iPrOx_{50\%})$, and (c) $P(EtOx_{75\%}iPrOx_{25\%})$) having different molecular weights (PEG standard, eluent: DMF (containing 10 mM LiCl and 30 mM TEA), temperature: 40 °C, RI detection).

The polymerization of Me-PEtOx-OH (8.763 g, 88.4 mmol) was also done under the synthetic conditions similar to that of Me-P*i*PrOx-OH with the initiation of methyl *p*-tosylate (MeOTs) (0.186 g, 1.0 mmol) in acetonitrile (30 mL) under mild temperature conditions (42 °C), followed by the treatment with

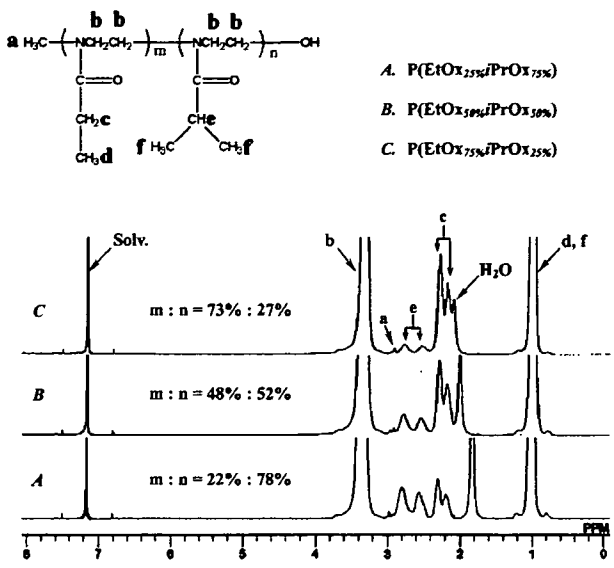

Figure 6. ^{1}H NMR spectra for the final products of three gradient copolymers (P(EtOx$_{25\%}$*i*PrOx$_{75\%}$), P(EtOx$_{50\%}$*i*PrOx$_{50\%}$), and P(EtOx$_{75\%}$*i*PrOx$_{25\%}$)) in $CDCl_3$ at 25 °C.

methanolic NaOH (1 M) for introducing a hydroxyl ω-end group. Under this condition, the polymerization should be left to proceed for ca. 315 h, but no noticeable side reactions occurred, as in the system of Me-P*i*PrOx-OH. It was confirmed from the GPC diagrams (Figure 2b) and MALDI-TOF mass spectra (Figure S2a−d) in the Supporting Information and Figure 3) that the polydispersity indices of all the sampling polymers including the final product were below 1.03, and the experimental M_n value ($M_{n,GPC}$ = 8000, $M_{n,TOF-MS}$ = 8300) was almost identical to the value predicted from the initial monomer/initiator ratio ($M_{n,calc}$ = 8800) (Table 1). The end-group analysis of the Me-PEtOx-OH was also done using the MALDI-TOF mass spectrum recorded after 315 h (Figure 3). The most intense signal can be assigned to the sodium adduct of Me-PEtOx-OH, while the second most intense signal is due to the lithium adduct of Me-PEtOx-OH. The ^{1}H NMR spectrum of Me-PEtOx-OH in $CDCl_3$ presented a broad singlet at 3.4 ppm attributed to the methylene protons of the polymer backbone, two broad singlets at 2.1−2.4 ppm, ascribed to methylene protons of the ethyl side chain and a broad singlet at 1.0 ppm due to the side chain methyl protons (Figure S3). To the best of our knowledge, this is the first demonstration of polymerizing an extremely monodispersive PEtOx homopolymers ($M_w/M_n \leq 1.02$) without inadvertent side reactions such as chain transfer and coupling,[16] often observed during the synthesis of conventional PEtOx systems under high-temperature conditions.[17]

The time-dependent monomer conversion obtained from the MALDI-TOF mass spectrometry for the respective polymerizations of both *i*PrOx and EtOx is also depicted in Figure 4, whereby the degree of polymerization (DP) was positioned at the left ordinate and the polydispersity index (PDI) (M_w/M_n) at the right ordinate. From the time-dependent DP and PDI changes of the two respective homopolymers, it was obvious that the polymerization rate of EtOx (●) was somewhat faster than that of *i*PrOx (◆) at 42 °C.

Synthesis of Gradient Copolymers. In view of the synthesis result of the two homopolymers described above, we planned to next synthesize a series of copolymers comprising EtOx and *i*PrOx in order to explore the hydrophilic contribution of EtOx on the LCST of P*i*PrOx (Scheme 1). The respective mixtures of 2-ethyl-2-oxazoline (EtOx$_{25\%}$: 2.19 g, 22.1 mmol; EtOx$_{50\%}$: 4.38 g, 44.2 mmol; EtOx$_{75\%}$: 6.57 g, 66.3 mmol) and 2-isopropyl-2-oxazoline (*i*PrOx$_{75\%}$: 7.5 g, 66.3 mmol; *i*PrOx$_{50\%}$: 5 g, 44.2 mmol; *i*PrOx$_{25\%}$: 2.5 g, 22.1 mmol) were added to a solution of MeOTs (0.186 g, 1.0 mmol) in acetonitrile (30 mL) and polymerized at 42 °C, as in the case of the two homopolymers (PEtOx and P*i*PrOx). The synthesis results of three copolymers (P(EtOx$_{25\%}$*i*PrOx$_{75\%}$), P(EtOx$_{50\%}$*i*PrOx$_{50\%}$), and P(EtOx$_{75\%}$*i*PrOx$_{25\%}$)) including two homopolymers with the same initial monomer/initiator ratio (DP$_{calc}$ = 88.4) are summarized in Table 1. The polymerization behaviors of the copolymers with the initial EtOx and *i*PrOx molar ratios of 25%:75%, 50%:50%, and 75%:25% were characterized by the time-dependent change in the DP and PDI via the MALDI-TOF mass and GPC traces, as seen in Figure 4. Regardless of the comonomer ratio in the feed, the experimental degree of polymerization (DP from MALDI-TOF mass spectrometry) of the respective copolymers was close to the predicted value from the initial monomer/initiator ratio (DP$_{calc}$ = 88.4) and their

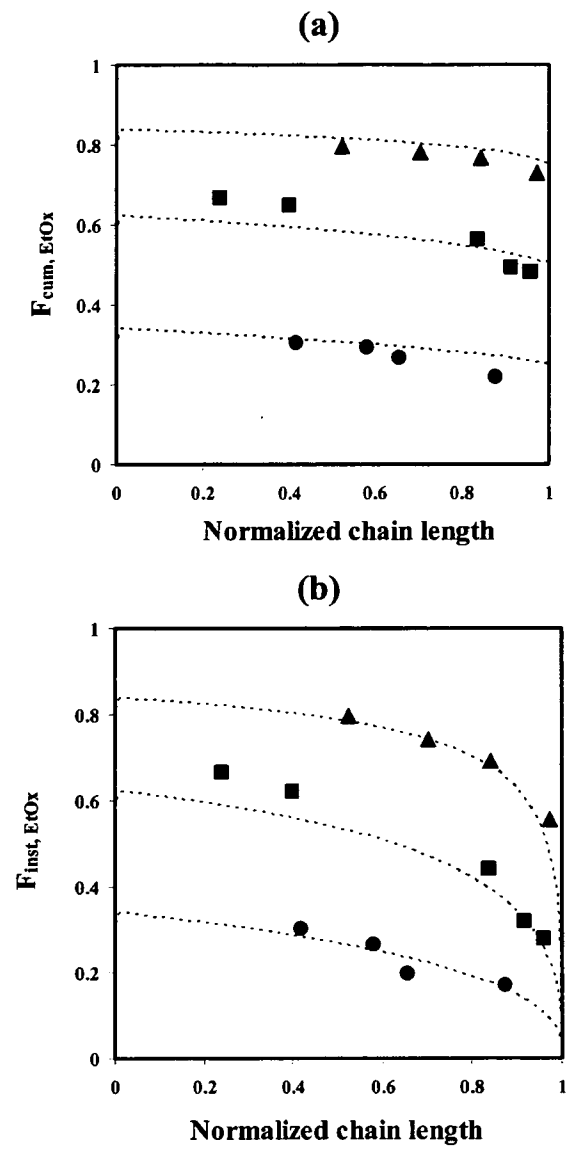

Figure 7. (a) Cumulative ($F_{cum,EtOx}$) and (b) instantaneous ($F_{inst,EtOx}$) composition plots for spontaneous gradient copolymers. The theoretical prediction curves (dotted) were calculated using the simulation program PROCOP[20] (P(EtOx$_{25\%}$*i*PrOx$_{75\%}$) (●), P(EtOx$_{50\%}$*i*PrOx$_{50\%}$) (■), and P(EtOx$_{75\%}$*i*PrOx$_{25\%}$) (▲)).

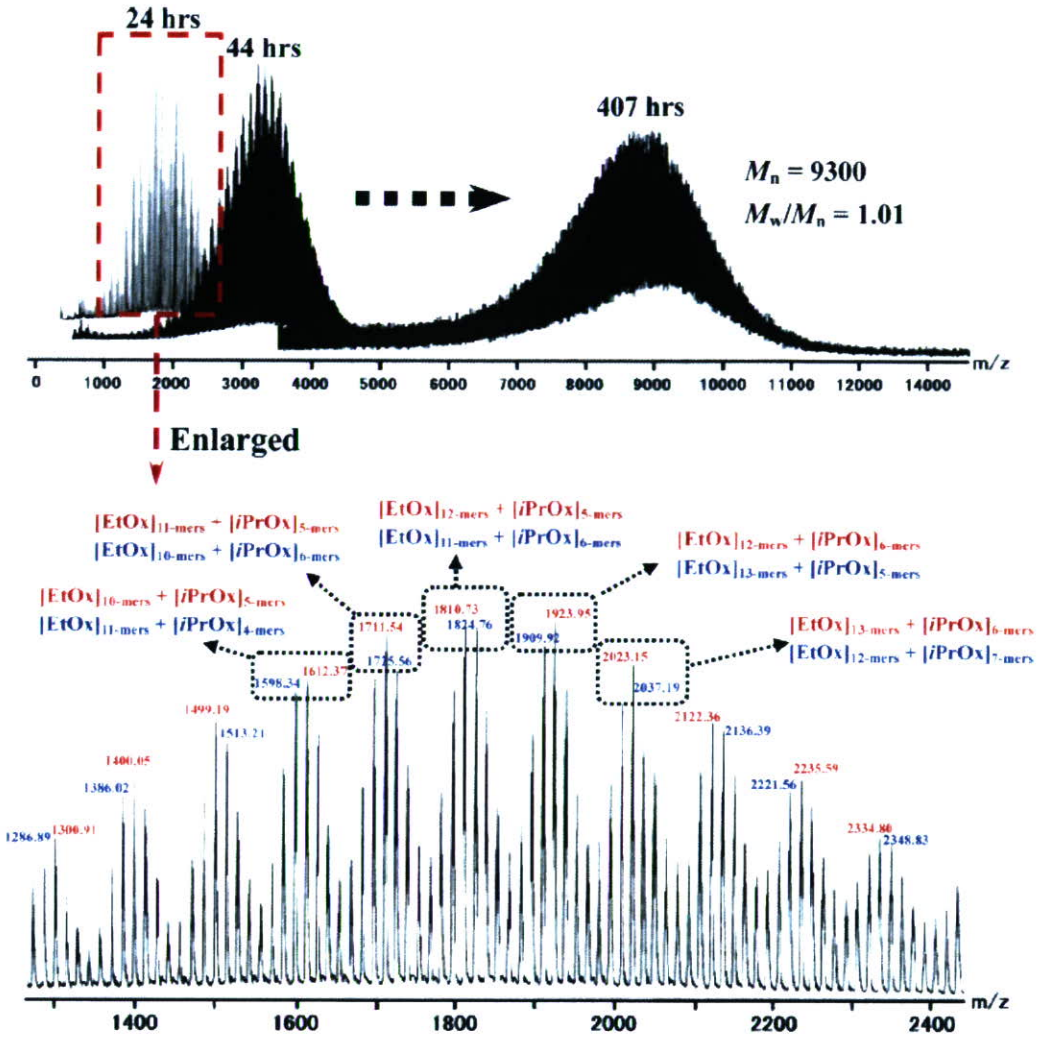

Figure 8. MALDI-TOF mass spectra of gradient copolymer samples comprising $EtOx_{50\%}$ and $iPrOx_{50\%}$ after 24, 44, and 407 h, respectively (upper), and enlarged detail in the mass region of 1300−2400 for the first sampling $P(EtOx_{50\%}iPrOx_{50\%})$ after 24 h (lower).

molecular weight distributions were appreciably narrow in all cases (Figure 4). The GPC traces of the three copolymers with different monomer ratios in the feed ($P(EtOx_{25\%}iPrOx_{75\%})$, $P(EtOx_{50\%}iPrOx_{50\%})$, and $P(EtOx_{75\%}iPrOx_{25\%})$), which were sampled at different polymerization times, also showed an increase in the molar mass with time and symmetrical monomodal peaks, as shown in Figure 5a−c. In addition, the compositions of the final copolymer products determined by ^1H NMR spectrometry were in good agreement with the calculated values from the feed ratio of both monomers, indicating their quantitative conversion into the respective copolymers (Figure 6 and Table 1).

In this living polymerization system, copolymers are expected to have a gradient composition, providing sufficiently different reactivity ratios of the two monomers, EtOx and *i*PrOx. Indeed, from the composition analysis by ^1H NMR spectrometry of the respective copolymer samplings (monomer conversions: ca. 20%−40%) plotted in Figure 4, the reactivity ratios of the respective monomers were calculated to be $r_{EtOx} = 1.78$ and $r_{iPrOx} = 0.79$ through the nonlinear Tidwell−Mortimer (TM) method, showing the most reasonable result among the well-established calculation methods for the further composition analysis of the copolymers (For the details on the determination of the reactivity ratios, see Tables S1 and S2 in the Supporting Information.) While in a conventional process the monomer reactivity ratios can be measured at low conversion (≤ca. 10%) with different monomer feeds, in the living process high polymer is not formed immediately in the reaction. Besides, measurements at such a low conversion could be also affected by the different reactivity of the initiator against a specific monomer. For this reason, the reactivity ratios should be calculated at comparatively higher monomer conversions (20% or higher).[13,18] As far as the polymerization of 2-oxazolines is concerned, it is also well-known that the initial polymerization rate can be different from the terminal polymerization rate,[19] so that we selected monomer conversions of ca. 20%−40% as a reasonable interval in this living system. This difference in the reactivity ratios of two monomers indicates that EtOx should initially be consumed much faster than *i*PrOx. However, because of the decreasing concentration of the former in the residual feed, the rate of its incorporation into the polymer chain also decreased. This resulted in an increased instantaneous incorporation of *i*PrOx into the copolymer as the reaction progressed and ultimately in the formation of an *i*PrOx-rich chain end. Because of the simultaneous initiation and uniform propagation kinetics in this living system as known from the appreciably low polydispersity indices ($M_w/M_n \leq 1.02$), each polymer chain should display a similar trend of a gradually decreasing EtOx and an increasing *i*PrOx composition along the backbone from the α-terminal to active ω-chain end. The cumulative and

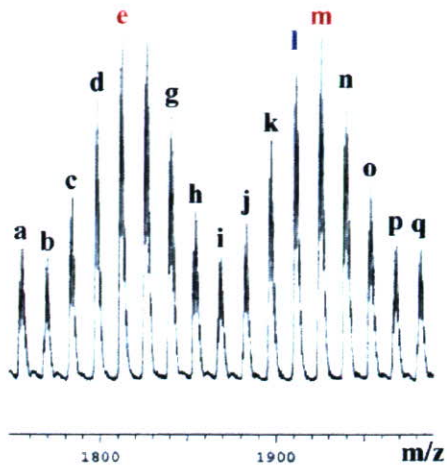

Assign.	$Mass_{calc.}$	$Mass_{exp.}$
a. $[EtOx]_{16\text{-mers}} + [iPrOx]_{1\text{-mers}}$	1754.270	1754.62
b. $[EtOx]_{15\text{-mers}} + [iPrOx]_{2\text{-mers}}$	1768.298	1768.65
c. $[EtOx]_{14\text{-mers}} + [iPrOx]_{3\text{-mers}}$	1782.326	1782.65
d. $[EtOx]_{13\text{-mers}} + [iPrOx]_{4\text{-mers}}$	1796.354	1796.69
e. $[EtOx]_{12\text{-mers}} + [iPrOx]_{5\text{-mers}}$	1810.382	1810.73
f. $[EtOx]_{11\text{-mers}} + [iPrOx]_{6\text{-mers}}$	1824.410	1824.76
g. $[EtOx]_{10\text{-mers}} + [iPrOx]_{7\text{-mers}}$	1838.438	1838.79
h. $[EtOx]_{9\text{-mers}} + [iPrOx]_{8\text{-mers}}$	1852.466	1852.83
i. $[EtOx]_{16\text{-mers}} + [iPrOx]_{2\text{-mers}}$	1867.428	1867.84
j. $[EtOx]_{15\text{-mers}} + [iPrOx]_{3\text{-mers}}$	1881.456	1881.87
k. $[EtOx]_{14\text{-mers}} + [iPrOx]_{4\text{-mers}}$	1895.484	1895.88
l. $[EtOx]_{13\text{-mers}} + [iPrOx]_{5\text{-mers}}$	1909.512	1909.92
m. $[EtOx]_{12\text{-mers}} + [iPrOx]_{6\text{-mers}}$	1923.540	1923.95
n. $[EtOx]_{11\text{-mers}} + [iPrOx]_{7\text{-mers}}$	1937.568	1937.99
o. $[EtOx]_{10\text{-mers}} + [iPrOx]_{8\text{-mers}}$	1951.596	1952.02
p. $[EtOx]_{9\text{-mers}} + [iPrOx]_{9\text{-mers}}$	1965.624	1966.05
q. $[EtOx]_{16\text{-mers}} + [iPrOx]_{3\text{-mers}}$	1980.586	1981.07

Figure 9. Enlarged detail of MALDI-TOF mass spectrum in the region of 1750−1990 (m/z) for gradient copolymer sample comprising $EtOx_{50\%}$ and $iPrOx_{50\%}$ after 24 h (left) and assignment of mass spectral peaks (right).

instantaneous composition plots ($F_{cum,EtOx}$ and $F_{inst,EtOx}$, respectively) vs the normalized chain length were obtained for the three copolymerizations with different initial molar ratios of EtOx and *i*PrOx in the feed (Figure 7). According to the plots, the shape of the obtained gradient copolymers closely followed the theoretical predictions using $r_{EtOx} = 1.78$ and $r_{iPrOx} = 0.79$.[20] In particular, the plots of the instantaneous composition vs normalized chain length showed the dependence of the gradient shapes on the initial feed composition. When the initial feed ratio of EtOx and *i*PrOx was varied from 75%:25% to 25%:75%, no significant continuous change in the instantaneous composition was observed, suggesting the gentle slope of the gradient along the copolymer main chain. The feasibility of this type of methodology has been well-known to trace the composition drift of gradient copolymers in the example of atom transfer radical polymerization (ATRP) living system.[13]

In addition, a series of MALDI-TOF mass spectra for $P(EtOx_{50\%}iPrOx_{50\%})$, which were sampled at different polymerization times, were obtained as shown in Figure 8, showing a good coincidence with the results of the GPC traces. When viewing the copolymers by mass spectra, the relative abundance of all the copolymers with a defined chain length reflects the information about the sequence and composition present in the copolymer.[21] The MALDI-TOF mass spectrometry thus provided a useful method to evaluate these two quantities with good precision, comparing the theoretical mass values and relative intensities for a specific copolymer with the experimental mass spectrum. The series of all the copolymer samplings with the chain lengths below ca. $M_n = 10\,000$ could provide comparatively clearer mass spectra, and the enlarged mass spectrum of $P(EtOx_{50\%}iPrOx_{50\%})$ sampled after 24 h was selected for the detailed analysis of copolymer composition and sequence distribution (Figure 8). All the peaks shown in the mass spectrum of Figure 8 were assigned to copolymers comprised of the EtOx and *i*PrOx monomer units with both methyl groups at the α-terminals and hydroxyl groups at the ω-terminals. The calculated mass of each copolymer is expressed by the following equation:

$$\begin{aligned} \text{mass}_{calc} &= [\text{EtOx}]_{m\text{-mers}} + [i\text{PrOx}]_{n\text{-mers}} \\ &= \Delta[\text{EtOx}]_m + \Delta[i\text{PrOx}]_n + \\ &[\alpha\text{-methyl and } \omega\text{-hydroxyl groups}] + [\text{Na}^+] \end{aligned}$$

where $mass_{calc}$ (m/z) is the calculated mass of a copolymer with degree of polymerization nearest the measured value, Δ[EtOx] (or Δ[*i*PrOx]) is the mass of the monomer unit, and $[Na^+]$ is the mass of a sodium ion. The detailed peak assignments are summarized in Table 2, where $mass_{exp}$ is the experimental mass value of the most and second intense signals among the respective homologue series in the mass region of 1300−2400. For instance, the strongest signal ($mass_{exp}$ = 1810.73) and second most intense signal ($mass_{exp}$ = 1824.76) in the mass region of 1750−1990 were in good agreement with the calculated mass values of the two corresponding copolymers, as shown below.

$$[\text{EtOx}]_{12-\text{mers}} + [i\text{PrOx}]_{5-\text{mers}} = 99.13 \times 12 + 113.158 \times 5 + 32.042 + 22.99 = 1810.382$$

$$[\text{EtOx}]_{11-\text{mers}} + [i\text{PrOx}]_{6-\text{mers}} = 99.13 \times 11 + 113.158 \times 6 + 32.042 + 22.99 = 1824.410$$

A more detailed assignment for all the mass spectral peaks in the region of 1750−1990 is also presented in Figure 9. Similar results for the other two gradient copolymers ($P(EtOx_{25\%}iPrOx_{75\%})$ and $P(EtOx_{75\%}iPrOx_{25\%})$) with different monomer ratios in the feed were also confirmed by MALDI-TOF mass spectrometry (Figures S4a−d and S5a−d in the Supporting Information).

In the case that the MALDI-TOF mass spectra were clearly recognized, the contour map exhibiting the number of *i*PrOx units per chain on the abscissa and the number of EtOx units per chain on the ordinate could be obtained by 2D plots using

Table 2. Assignment of MALDI-TOF Mass Spectral Peaks Shown in Figure 8

assignt	$mass_{calc}$	$mass_{exp}$	assignt	$mass_{calc}$	$mass_{exp}$
$[EtOx]_{8-mers} + [iPrOx]_{4-mers}$	1300.704	1300.91	$[EtOx]_{9-mers} + [iPrOx]_{3-mers}$	1286.676	1286.89
$[EtOx]_{9-mers} + [iPrOx]_{4-mers}$	1399.834	1400.05	$[EtOx]_{10-mers} + [iPrOx]_{3-mers}$	1385.806	1386.02
$[EtOx]_{10-mers} + [iPrOx]_{4-mers}$	1498.964	1499.19	$[EtOx]_{9-mers} + [iPrOx]_{5-mers}$	1512.992	1513.21
$[EtOx]_{10-mers} + [iPrOx]_{5-mers}$	1612.122	1612.37	$[EtOx]_{11-mers} + [iPrOx]_{4-mers}$	1598.094	1598.34
$[EtOx]_{11-mers} + [iPrOx]_{5-mers}$	1711.252	1711.54	$[EtOx]_{10-mers} + [iPrOx]_{6-mers}$	1725.280	1725.56
$[EtOx]_{12-mers} + [iPrOx]_{5-mers}$	1810.382	1810.73	$[EtOx]_{11-mers} + [iPrOx]_{6-mers}$	1824.410	1824.76
$[EtOx]_{12-mers} + [iPrOx]_{6-mers}$	1923.540	1923.95	$[EtOx]_{13-mers} + [iPrOx]_{5-mers}$	1909.512	1909.92
$[EtOx]_{13-mers} + [iPrOx]_{6-mers}$	2022.670	2023.15	$[EtOx]_{12-mers} + [iPrOx]_{7-mers}$	2036.698	2037.19
$[EtOx]_{14-mers} + [iPrOx]_{6-mers}$	2121.800	2122.36	$[EtOx]_{13-mers} + [iPrOx]_{7-mers}$	2135.828	2136.39
$[EtOx]_{14-mers} + [iPrOx]_{7-mers}$	2234.958	2235.59	$[EtOx]_{15-mers} + [iPrOx]_{9-mers}$	2220.930	2221.56
$[EtOx]_{15-mers} + [iPrOx]_{7-mers}$	2334.088	2334.80	$[EtOx]_{14-mers} + [iPrOx]_{8-mers}$	2348.116	2348.83

Microsoft Excel 2002 software.[22] After completing the precise mass assignment of all the peaks in the region of 1300−2400 (m/z) for the $P(EtOx_{50\%}iPrOx_{50\%})$ sampling after 24 h, the contribution of each monomer unit to the calculated mass value of a copolymer with the degree of polymerization to nearest the measured value was determined, and the relative abundance (or intensity) of the assigned copolymer was represented as a function of the number of EtOx and *i*PrOx units (Figure 10a). From this 2D graph, it was obvious that the amount of EtOx in the copolymer backbone was ca. twice that of *i*PrOx during the initial period of copolymerization (24 h), which was caused by the sufficiently different reactivity ratios of the two monomers. Furthermore, the six contour maps after 24, 44, 70, 168, 265, and 407 h are also represented on the single $x-y$ coordinate system with the similar treatments (Figure 10b). Since it was hard to consider all the mass regions of the copolymer, the specific intervals within the seven lines and seven columns centering on the most intense signals should be selectively exhibited for clarification. The traces of all the contour maps were in good agreement with the result of the composition analysis of the two monomer units by ^1H NMR spectrometry as shown in Figure S6 of the Supporting Information.

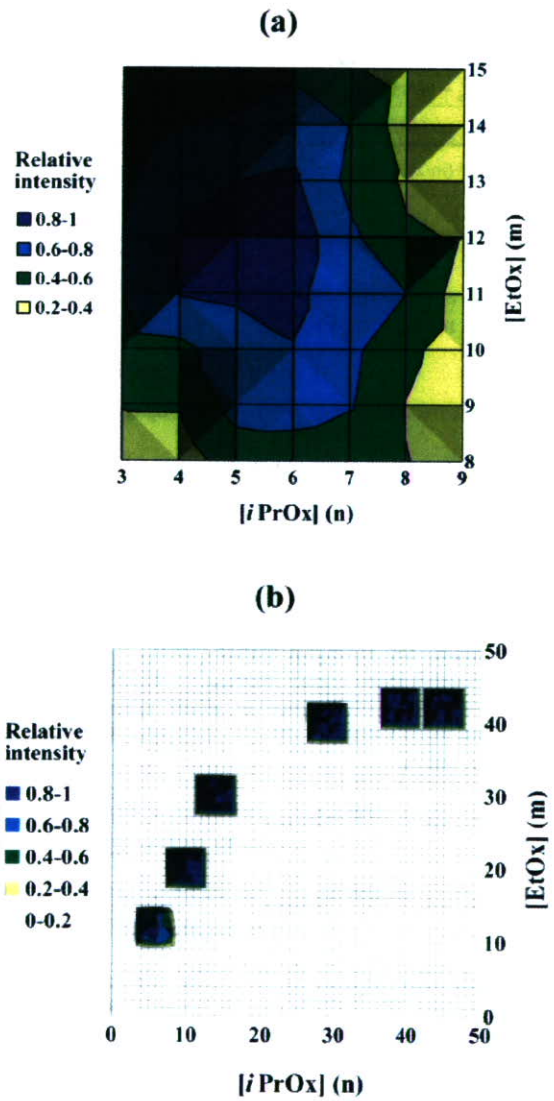

Figure 10. Gradient copolymer fingerprint obtained from MALDI-TOF mass analysis: a contour map showing the number of *i*PrOx units on the abscissa and the number of EtOx units on the ordinate (a) in the mass region of 1300−2400 for the first sampling $P(EtOx_{50\%}iPrOx_{50\%})$ after 24 h and (b) trace of six contour maps obtained after 24, 44, 70, 168, 265, and 407 h.

Determination of the Cloud Points (T_{cp}). The measurement of the changing points in turbidity, defined here as the cloud points (T_{cp}), was adapted to determine the lower critical solution temperature (LCST) of a polymer solution. Figure 11a shows the dependence of the turbidity on the increasing temperature for the (co)polymer solutions with a different EtOx composition. The transmittance sharply decreased at a specific temperature in phosphate-buffered solution (10 mM PBS (pH = 7.4)) in

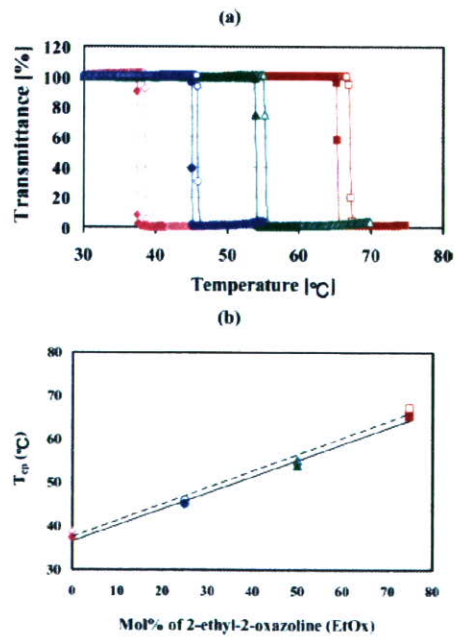

Figure 11. (a) Transmittance changes at 500 nm of 1.0 wt % (co)-polymer solutions (*Pi*PrOx (◆, ◇), $P(EtOx_{25\%}iPrOx_{75\%})$ (●, ○), $P(EtOx_{50\%}iPrOx_{50\%})$ (▲, △), and $P(EtOx_{75\%}iPrOx_{25\%})$ (■, □)) as a function of temperature (10 mM PBS (pH = 7.4) in the absence (open shape) or presence (closed shape) of 150 mM NaCl, rate 0.5 °C/min). (b) Relationship between cloud point (T_{cp}) and comonomer (EtOx) composition in the (co)polymers.

the absence (open symbols) or presence (closed symbols) of 150 mM NaCl, indicating a sharp LCST-type phase transition. The LCST values were found to linearly increase with the increasing mol % of EtOx (n), from 38.7 °C (or 37.4 °C) at n = 0% to 67.3 °C (or 65.4 °C) at n = 75% for a 1.0 wt % polymer solution in the absence (or presence) of 150 mM NaCl (Figure 11b). Regardless of the *i*PrOx to EtOx ratio, an exceedingly clear sensitivity of the phase separation was observed in all cases, whereas no change in transmittance appeared in the case of a PEtOx homopolymer at the measured temperatures up to 90 °C (Table 1). It was also observed that the LCST values of the (co)polymer solutions in the presence of 150 mM NaCl, viz., near the physiological condition, slightly shifted to lower temperatures in all cases compared to that in the absence of NaCl. This result was in agreement with the well-known "salting-out" effect of NaCl.[23]

A notable point of these turbidity results is that observed transition was appreciably sharp and simply correlated with the ratio of both monomers in the copolymers even though they have the compositional gradient along the polymer strand. It may be reasonable to assume that the LCST property of such a gradient copolymer may become complicated due to a possible formation of micelle-like molecular association derived from a deviating amphiphilicity along the polymer chain. Nevertheless, the static light scattering (SLS) measurements of the solution with varying temperature provided no obvious sign of assembly formation, keeping the weak and constant scattering intensity up to the LCST (data not shown). Although we may not exclude the possibility of conformational change in a single strand of the gradient copolymers below LCST due to the deviating amphiphilicity in the strand, turbidity behavior follows a rather simple and practical rule to be correlated with the ratio of both monomers in the copolymers. Detailed solution behavior of these gradient copolymers should be an important topic for the further study to understand their actual molecular dynamics related to temperature change, yet the present study recalls the well-established oxazoline polymerization as a convenient procedure to obtain the copolymers with extremely narrow molecular weight distribution and finely tuned LCST.

Conclusions

This study developed the facile and precise synthetic route of thermosensitive POx gradient copolymers via the living cationic polymerization of 2-isopropyl-2-oxazoline (*i*PrOx) mixed with a specific composition of 2-ethyl-2-oxazoline (EtOx) as a hydrophilic comonomer. The oxazoline monomers (EtOx and *i*PrOx) had sufficiently different reactivity ratios of 1.78 and 0.79, respectively, leading to obtain the gradient copolymers with varying composition and very narrow molecular weight distribution. Turbidity measurements revealed that LCST of the gradient copolymers can be minutely modulated over a broad range of temperature from 38.7 to 67.3 °C simply by varying the molar ratio of EtOx to *i*PrOx. This approach of copolymerizing a variety of oxazoline monomers with different hydrophobic and hydrophilic balance, in a condition to attain living polymerization (mild temperature in acetonitrile), apparently lead to the systematic preparation of versatile end-functionalized polyoxazoline derivatives with finely tuned LCST, which have a promising feasibility particularly in biomedical applications as constructing thermosensitive bioconjugates and drug delivery systems.

Acknowledgment. This work was financially supported by Special Coordination Funds for Science and Technology from the Ministry of Education, Culture, Sports, Science and Technology of Japan (MEXT) as well as by the Core Research for Evolutional Science and Technology (CREST) from the Japan Science and Technology Agency (JST).

Supporting Information Available: Figures S1−S6 and Tables S1 and S2. This material is available free of charge via the Internet at http://pubs.acs.org.

References and Notes

(1) (a) Bergbreiter, D. E.; Osburn, P. L.; Wilson, A.; Sink, E. M. *J. Am. Chem. Soc.* **2000**, *122*, 9058. (b) Hamamoto, H.; Suzuki, Y.; Yamada, Y.; Tabata, H.; Takahashi, H.; Ikegami, S. *Angew. Chem., Int. Ed.* **2005**, *44*, 4536.

(2) (a) Uchiyama, S.; Kawai, N.; de Silva, A. P.; Iwai, K. *J. Am. Chem. Soc.* **2004**, *126*, 3032. (b) Hu, Z. B.; Chen, Y. Y.; Wang, C. J.; Zheng, Y. D.; Li, Y. *Nature (London)* **1998**, *393*, 149.

(3) (a) Kanazawa, H.; Yamamoto, K.; Matsushima, Y.; Takai, N.; Kikuchi, A.; Sakurai, Y.; Okano, T. *Anal. Chem.* **1996**, *68*, 100. (b) Kikuchi, A.; Okano, T. *Prog. Polym. Sci.* **2002**, *27*, 1165.

(4) (a) Stayton, P. S.; Shimoboji, T.; Long, C.; Chilkoti, A.; Chen, G.; Harris, J. M.; Hoffman, A. S. *Nature (London)* **1995**, *378*, 472. (b) Matsukata, M.; Aoki, T.; Sanui, K.; Ogata, N.; Kikuchi, A.; Sakurai, Y.; Okano, T. *Bioconjugate Chem.* **1996**, *7*, 96. (c) Ding, Z.; Chen, G.; Hoffman, A. S. *J. Biomed. Mater. Res.* **1998**, *39*, 498.

(5) (a) Yoshida, R.; Sakai, T.; Okano, T.; Sakurai, Y.; Bae, Y. H.; Kim, S. W. *J. Biomater. Sci., Polym. Ed.* **1991**, *3*, 155. (b) Cammas, S.; Suzuki, K.; Sone, Y.; Kakurai, Y.; Kataoka, K.; Okano, T. *J. Controlled Release* **1997**, *48*, 157. (c) Kono, K. *Adv. Drug. Deliv. Rev.* **2001**, *53*, 307.

(6) (a) Park, J. S.; Akiyama, Y.; Winnik, F. M.; Kataoka, K. *Macromolecules* **2004**, *37*, 6786. (b) Diab, C.; Akiyama, Y.; Kataoka, K.; Winnik, F. M. *Macromolecules* **2004**, *37*, 2556.

(7) (a) Kobayashi, S. *Prog. Polym. Sci.* **1990**, *15*, 751. (b) Aoi, K.; Okada, M. *Prog. Polym. Sci.* **1996**, *21*, 151. (c) Kobayashi, S.; Uyama, H. *J. Polym. Sci., Part A: Polym. Chem.* **2002**, *40*, 192.

(8) (a) Heskins, M.; Guillent, J. E.; James, E. J. *J. Macromol. Sci., Chem.* **1968**, *A2*, 1441. (b) Schild, H. G. *Prog. Polym. Sci.* **1992**, *17*, 163.

(9) (a) Woodle, M. C.; Engbers, C. M.; Zalipsky, S. *Bioconjugate Chem.* **1994**, *5*, 493. (b) Zalipsky, S.; Hansen, C. B.; Oaks, J. M.; Allen, T. M. *J. Pharm. Sci.* **1996**, *85*, 133.

(10) (a) Taylor, L. D.; Cerankowski, L. D. *J. Polym. Sci.* **1975**, *13*, 2551. (b) Feil, H.; Bae, Y. H.; Feijen, J.; Kim, S. W. *Macromolecules* **1993**, *26*, 2496.

(11) (a) Sugihara, S.; Kanaoka, S.; Aoshima, S. *Macromolecules* **2004**, *37*, 1711. (b) Ali, M. M.; Stöver, H. D. H. *Macromolecules* **2004**, *37*, 5219. (c) Mori, H.; Iwaya, H.; Nagai, A.; Endo, T. *Chem. Commun.* **2005**, *38*, 4872. (d) Lutz, J.; Hoth, A. *Macromolecules* **2006**, *39*, 893.

(12) (a) Kagiya, T.; Matsuda, T.; Nakato, M.; Hirata, R. *J. Macromol. Sci., Chem.* **1972**, *6*, 1631. (b) Cai, G.; Litt, M. *J. Polym. Sci., Part A: Polym. Chem.* **1992**, *30*, 649. (c) Hoogenboom, R.; Fijten, M. W. M.; Schubert, U. S. *J. Polym. Sci., Part A: Polym. Chem.* **2004**, *42*, 1830.

(13) (a) Pakula, T.; Matyjaszewski, K. *Macromol. Theory Simul.* **1996**, *5*, 987. (b) Matyjaszewski, K.; Ziegler, M. J.; Arehart, S. V.; Greszta, D.; Pakula, T. *J. Phys. Org. Chem.* **2000**, *13*, 775.

(14) Seeliger, W.; Aufderhaar, E.; Diepers, W.; Feinauer, R.; Nehring, R.; Their, W.; Hellmann, H. *Angew. Chem., Int. Ed. Engl.* **1966**, *5*, 875.

(15) Perrin, D. D.; Armarego, W. L. F.; Perrin, D. R. *Purification of Laboratory Chemicals*; Pergamon: Oxford, 1980.

(16) (a) Levy, A.; Litt, M. *J. Polym. Sci., Part A-1* **1968**, *6*, 1883. (b) Litt, M.; Levy, A.; Herz, J. *J. Macromol. Sci., Chem.* **1975**, *A9*, 703. (c) Warakomski, J. M.; Thill, B. P. *J. Polym. Sci., Part A* **1990**, *28*, 3551.

(17) (a) Liu, Q.; Konas, M.; Riffle, J. S. *Macromolecules* **1993**, *26*, 5572. (b) Chen, C. H.; Wilson, J.; Chen, W.; Davis, R. M.; Riffle, J. S. *Polymer* **1994**, *35*, 3587. (c) Kobayashi, S.; Masuda, E.; Shoda, S.; Shimano, Y. *Macromolecules* **1989**, *22*, 2878. (d) Wiesbrock, F.; Hoogenboom, R.; Leenen, M. A. M.; Meier, M. A. R.; Schubert, U. S. *Macromolecules* **2005**, *38*, 5025.

(18) Madruga, E. L. *Prog. Polym. Sci.* **2002**, *27*, 1879.

(19) (a) Saegusa, T.; Ikeda, H.; Fujii, H. *Macromolecules* **1973**, *6*, 315. (b) Saegusa, T.; Kobayashi, S.; Yamada, A. *Makromol. Chem.* **1976**, *177*, 2271. (c) Uyama, H.; Kobayashi, S. *Macromolecules* **1991**, *24*, 614.

(20) Hagipol, C. *Copolymerization-Toward a Systematic Approach*; Kluwer Academic: New York, 1999.

(21) (a) Montaudo, M. S. *Rapid Commun. Mass Spectrom.* **1999**, *13*, 639. (b) Montaudo, M. S. *Mass Spectrom. Rev.* **2002**, *21*, 108.

(22) Terrier, P.; Buchmann, W.; Cheguillaume, G.; Desmazières, B.; Tortajada, J. *Anal. Chem.* **2005**, *77*, 3292.

(23) Lin, P.; Pearce, E. M.; Kwei, T. K. *J. Polym. Sci., Part B: Polym. Phys.* **1988**, *26*, 603.

MA0605548

Mod Rheumatol (2006) 16:24–29
DOI 10.1007/s10165-005-0450-6

ORIGINAL ARTICLE

**Noriko Yoshimura · Hirofumi Kinoshita · Noriaki Hori
Taira Nishioka · Masahiko Ryujin · Yoshihiko Mantani
Mariko Miyake · Tatsuya Takeshita · Masao Ichinose
Munehito Yoshiida · Hiroyuki Oka · Hiroshi Kawaguchi
Kozo Nakamura · Cyrus Cooper**

Risk factors for knee osteoarthritis in Japanese men: a case-control study

Received: July 27, 2005 / Accepted: December 13, 2005

Abstract Risk of knee osteoarthritis (OA) was assessed in a population-based case-control study of Japanese men. The study covered three health districts in Wakayama and Osaka prefectures, Japan. Subjects were male individuals ≥45 years old diagnosed radiographically with knee OA, and who did not display any established causes of secondary OA. Controls selected randomly from the general population were individually matched to cases for age, sex, and residential district. Subjects were interviewed using structured questionnaires to determine medical history, physical activity, socio-economic factors, and occupation. Interviews were obtained from 37 cases and 37 controls. In univariate analysis, heaviest weight in the past and physical work such as factory, construction, agricultural, or fishery work as the principal occupation significantly raised the risk of male knee OA ($P < 0.05$). Odds ratios (OR) were determined using conditional logistic regression analysis mutually adjusted for potential risk factors using the results of univariate analysis. Heaviest weight in the past (OR 6.01, 95% confidence interval (CI) 1.18–30.5, $P < 0.05$), past knee injury (OR 6.25, 95% CI 1.13–34.5, $P < 0.05$), and physical work as the principal occupation (OR 6.20, 95% CI 1.40–27.5, $P < 0.05$) represented independent factors associated with knee OA after controlling for other risk factors. Physical work is associated with knee OA, demonstrating the influence of working activity on the development of OA. The present study suggests that risk factors for knee OA in men resemble those in women.

Key words Case control study · Heavy weight · Knee joint · Osteoarthritis (OA) · Physical work

N. Yoshimura (✉) · H. Oka
Department of Joint Disease Research, Graduate School of Medicine, The University of Tokyo, 7-3-1 Hongo, Bunkyo-ku, Tokyo 113-8655, Japan
Tel. +81-3-5800-9178; Fax +81-3-5800-9179
e-mail: yoshimuran-ort@h.u-tokyo.ac.jp

H. Kinoshita
Department of Orthopaedic Surgery, Wakayama Medical University Kihoku Hospital, Wakayama, Japan

N. Hori
Hori Hospital, Sennan, Japan

T. Nishioka
Nishioka Orthopaedic Hospital, Arita, Japan

M. Ryujin
Ryujin Clinic, Wakayama, Japan

Y. Mantani
Tamai Orthopaedic Hospital, Hannan, Japan

M. Miyake
Yamomoto Clinic, Shimotsu, Japan

T. Takeshita
Department of Public Health, Wakayama Medical University School of Medicine, Wakayama, Japan

M. Ichinose
Second Department of Internal Medicine, Wakayama Medical University School of Medicine, Wakayama, Japan

M. Yoshiida
Department of Orthopaedic Surgery, Wakayama Medical University School of Medicine, Wakayama, Japan

H. Kawaguchi · K. Nakamura
Department of Orthopaedic Surgery, Faculty of Medicine, The University of Tokyo, Tokyo, Japan

C. Cooper
MRC Epidemiology Resource Centre, University of Southampton, Southampton General Hospital, Southampton, UK

Introduction

Since osteoarthritis (OA) is a frequent cause of pain and disability in elderly individuals, the recent World Health Organization report on the global burden of disease indicated knee OA as an increasingly important cause of disability in both men and women, suggesting that strategies for preventing OA are urgently required.[1] In Japan, knee OA seems to represent a frequent cause of pain and disability, but few epidemiological studies have examined associated factors.

Several investigations regarding risk factors for hip and knee OA performed in Western populations have

suggested obesity, previous injury, polyarticular joint involvement, and occupational activities as important risk factors for the disorder.[2-8] However, few studies of risk factors for OA in Japanese populations have been performed. Our earlier case-control study of hip OA identified some variations in risk factors in Japan.[9] In the previous case-control study of hip OA, occupational lifting was identified as a risk factor and sedentary work as a protective factor for hip OA. In addition, obesity was not identified as a risk factor for Japanese hip OA. For contrast, an identical case-control study was performed for knee OA in women in a Japanese population.[10] In the female study, risk factors of obesity, previous knee injury, and period of total work were identified, and sedentary work as the initial occupation represented a preventive factor.[10] The results from these two investigations suggest various similarities and differences in risk factors between hip and knee OA in Japanese populations.

The present study sought to clarify risk factors for knee OA among men in Japan, by performing a survey identical to that used in the previous female knee OA study. Results for men were compared to those from the female study.[10] Risk factors were then compared between knee OA and hip OA to address differences in risk factors for constitutional and mechanical factors between OA at different sites. Finally, risk factors for knee and hip OA were compared to those identified in a British study[11,12] that used identical methods to the Japanese studies, to clarify differences in risk factors for OA between Japanese and Western populations.

Patients and methods

Methods of data collection in the present study were basically identical to those of the case-control studies for female knee OA and hip OA reported previously.[9,10] A brief summary is provided here. Cases were identified from the registration systems of the six hospitals participating in the study, which were located in three cities in Japan (Wakayama City and Arita City in Wakayama Prefecture, and Sennan City in Osaka Prefecture).

Cases comprised men ≥45 years old who suffered knee pain and walking difficulties, and who were first diagnosed by an orthopedic surgeon as displaying a tibiofemoral joint with radiographic grade of ≥3 on the Kellgren and Lawrence scale[13] within the year preceding the start of the study. Cases with a history of knee injury in the previous year, rheumatoid arthritis, or ankylosing spondylitis were excluded.

For each case, a single control was randomly selected from among men of the same age and district of residence on city registers of the local population, which are updated as residents move into or leave the city. Controls who had suffered knee OA were excluded from the study.

All eligible cases and controls were initially approached using a letter to determine willingness to participate in the study. After providing informed consent, cases and controls were interviewed by the same trained interviewer.

An identical questionnaire to that used in the British case-control study was used to ascertain risk factors of knee OA.[11,12] The questionnaire was translated and back-translated from Japanese to English. Subjects completed a structured questionnaire that requested details of medical history, socio-economic status and education, cigarette smoking and alcohol consumption, functional status, and lifetime history of leisure activities. Lifetime history of leisure activities included participation in sports such as soccer, swimming, tennis, cricket, and golf, in addition to frequency and duration of less physical activities, such as gardening. Information about eight types of occupational physical activity was requested, namely: standing; sitting; climbing stairs; kneeling; squatting; driving; walking; and heavy lifting. Information on these activities was obtained for the initial job, defined as the earliest job reported, and for the principal job, defined as the job at which the subject had worked longest. For each job, the questionnaire enquired whether work entailed lifting weights (≥10 kg, ≥25 kg, or ≥50 kg) more than once during an average working week. Information regarding use of transport, including frequency and duration of cycling and motorcycling was obtained. Information was also requested on the involvement of other joints, including hands, shoulders, and hips. Furthermore, questions were added about back pain and stiffness, which were not included in the British study. Once heaviest reported weight after 25 years old was obtained, height and weight of each subject was measured at the time of the interview.

After analysis to clarify risk for male knee OA, results were compared between men and published results for women.[10] Risk factors for knee OA and hip OA were also compared to address differences in constitutional and mechanical risk factors between OA at different sites. Finally, risk factors for knee and hip OA were compared to the findings of the British study, which used identical methods to the Japanese studies.

Data were calculated using McNemar's Chi-square test and conditional logistic regression tests for matched sets. Results were summarized as odds ratios (OR) with 95% confidence intervals (CI). Odds ratios were calculated for categories of exposure, and tests of trend were performed across these categories. Statistical analyses were performed using SPSS statistical software (SPSS, Chicago, IL, USA) and the STATA statistical package (STATA, College Station, TX, USA).

Results

A total of 40 men ≥45 years old fulfilled the entry criteria for the study. Among these eligible cases, 37 men (92.5%) agreed to participate after information was provided. Unilateral knee OA (n = 21) was more common than bilateral disease (n = 16). Among the 21 men with unilateral disease, OA tended to be right-sided (n = 13) more often

than left-sided (n = 8), but no significant difference was identified.

For controls, we approached age-, sex-, and residence-matched candidates for each case. To recruit the 37 matched controls, we approached 70 subjects (overall response rate 52.9%).

Table 1 shows background characteristics for the 37 case-control pairs in the present study. Mean body weight was significantly greater for cases than for controls ($P < 0.05$). Furthermore, body mass index was significantly higher for cases than for controls ($P < 0.05$). No differences in personal habits such as smoking or drinking were noted between cases and controls.

The association between knee OA and heaviest reported body weight was analyzed. Under univariate analysis, mean heaviest reported body weight for cases was 72.1 kg (standard deviation (SD) = 13.0 kg), significantly higher than that for controls ($P < 0.01$) in men. Odds ratios for heaviest reported body weight were 1.07 (95% CI 1.02–1.13), suggesting that a 1-kg increase in heaviest reported body weight raised the risk of knee OA by 7%.

To more clearly address the influence of heaviest reported weight on development of knee OA, cases were categorized into the following three groups according to the distribution of heaviest reported weight: high, ≥72.0 kg; middle, 61.0–72.0 kg; and low, <61.0 kg. These categories were defined by dividing total distributions into equal thirds. Cases in the high group displayed a >4-fold elevation in risk compared with cases in the low group (OR 4.22, 95% CI 1.13–15.8 for high vs low, $P < 0.05$; OR 1.60, 95% CI 0.50–5.08 for middle vs low, $P = 0.43$) (Fig. 1).

The association between knee OA and history of injury in other joints was calculated. Under univariate analysis, although ORs exceeded a 2-fold increase, no significant difference was observed between cases and controls (OR 2.50, 95% CI 0.78–7.97 for yes vs no, $P = 0.12$).

The association between knee OA and methods of transportation was examined by comparing the frequency of regular bicycle use between cases and controls. Under univariate analysis, while OR was higher for men (OR 2.67, 95% CI 0.71–10.05), no significant differences were noted between cases and controls.

Associations between knee OA and occupational history were analyzed. The most frequent areas of employment for all subjects were factory/construction, agriculture/fishery, clerical/technical, and shop assistant/manager (Table 2). Distributions of initial and principal occupations differed

Table 1. Anthropometric and background characteristics of cases and controls for knee OA in men

	Men	
	Cases	Controls
No. of participants	37	37
Age (years)	70.0 ± 6.6	70.1 ± 7.0
Weight (kg)	64.1 ± 10.7*	59.3 ± 8.7
Height (cm)	162.5 ± 6.9	163.0 ± 6.7
Body mass index (kg/m^2)	24.2 ± 3.4*	22.4 ± 3.8
Heaviest weight in the past (kg)	72.1 ± 13.0**	64.0 ± 9.2
Age at the heaviest weight (years)	57.4 ± 15.1*	51.7 ± 17.8
Current smoking (%)	16 (43.2)	15 (40.5)
Current drinking (≥5 times/week, %)	20 (54.1)	22 (59.5)

Mean ± SD; percentage in parentheses
* $P < 0.05$, ** $P < 0.01$ cases vs controls

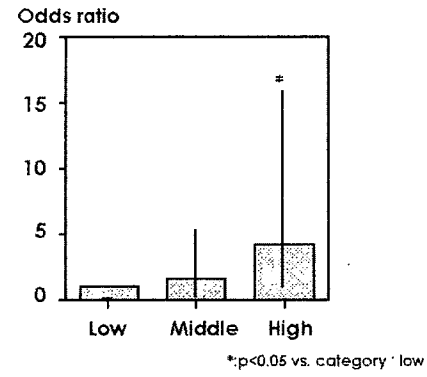

Fig. 1. Association of knee osteoarthritis with heaviest weight in the past. *Low*, lowest 3rd of the heaviest weight category, <61.0 kg; *Middle*, middle 3rd, ≥61.0 kg, <72.0 kg; *High*, highest 3rd, ≥72.0 kg. *Bar* represents 95% confidence interval

Table 2. Occupations reported as initial and principal jobs in men

	Initial occupation				Principal occupation			
	Cases	%	Controls	%	Cases	%	Controls	%
Total	37	100	37	100	37	100	37	100
Factory/construction workers	18	48.6	14	37.8	22	59.5	16	43.2
Agricultural/fishery workers	10	27.0	6	16.2	7	18.9	4	10.8
Clerical workers/technical experts	4	10.8	6	16.2	2	5.4	9	24.3
Shop assistants and managers	2	5.4	9	24.3	2	5.4	6	16.2
Clinical workers	2	5.4	0	0.0	1	2.7	0	0.0
Housekeepers	0	0.0	0	0.0	0	0.0	0	0.0
Hairdressers	0	0.0	0	0.0	0	0.0	0	0.0
Dressmakers	0	0.0	0	0.0	0	0.0	0	0.0
Teachers	0	0.0	0	0.0	2	5.4	0	0.0
Others (soldier, taxi driver, etc.)	1	2.7	2	5.4	1	2.7	2	5.4
No work, no answer	0	0.0	0	0.0	0	0.0	0	0.0

Table 3. Crude and adjusted odds ratios with risk factors for knee osteoarthritis in men

Men	Risk factors	Crude odds ratio (95% CI)	Adjusted odds ratio (95% CI)
Heaviest reported weight[a]	Middle vs Low	1.60 (0.50–5.08)	1.25 (0.29–5.35)
	High vs Low	4.22 (1.13–15.8)*	6.01 (1.18–30.5)*
Past injury of either knee	Yes vs No	2.50 (0.78–7.97)	6.25 (1.13–34.5)*
Occupational factors	Physical work[b] as principal occupation (vs Others)	2.80 (1.01–7.77)*	6.20 (1.40–27.5)*

Adjusted odds ratio refers to values after mutual adjustment for other potential risk estimates
95% CI, 95% confidence interval
[a]Lowest 3rd, <61.0 kg; middle 3rd, ≥61.0 kg, <72.0 kg; highest 3rd, ≥72.0 kg in men
[b]Physical work meaning factory, construction, agriculture or fishery work
* $P < 0.05$

Table 4. Crude and adjusted odds ratios with risk factors for knee osteoarthritis in women (cited from ref. 10)

Women	Risk factors	Crude odds ratio (95% CI)	Adjusted odds ratio (95% CI)
Heaviest reported weight[a]	Middle (vs Low)	1.68 (0.79–3.84)	3.33 (0.95–11.7)
	High (vs Low)	3.10 (1.26–7.98)*	3.92 (1.03–14.8)*
Past injury of either knee	Yes vs No	5.00 (2.44–10.2)*	7.51 (2.40–23.5)**
Transportation	Cycling almost every day for ≥12 months (vs Less)	1.88 (1.02–3.94)*	1.67 (0.61–4.57)
Occupational factors	Physical work[b] as initial occupation (vs Others)	2.54 (1.34–4.82)**	2.08 (0.88–5.61)
	Sitting ≥2 h/day at initial job (vs Less)	0.43 (0.23–0.78)**	0.44 (0.47–1.10)
	No. of jobs (1 job)	1.24 (1.02–1.50)*	0.91 (0.66–1.25)
	Total working period (1 year)	1.05 (1.03–1.07)***	1.05 (1.01–1.08)**

Adjusted odds ratio refers to values after mutual adjustment for other potential risk estimates
95% CI, 95% confidence interval
[a]Lowest 3rd, <55.0 kg; middle 3rd, ≥55.0 kg, <62.0 kg; highest 3rd, ≥62.0 kg in women
[b]Physical work meaning factory, construction, agriculture or fishery work
* $P < 0.05$; ** $P < 0.01$; *** $P < 0.001$

significantly between cases and controls. Physical work (factory/construction or agriculture/fishery) at the principal job was significantly more common among cases than controls (OR 2.80, 95% CI 1.01–7.77 for yes vs no). Mean age at commencement of the first job was 16.3 years (SD 3.8 years) compared to 16.6 years (SD 4.1 years) for controls, indicating no significant difference between cases and controls. Occupational activities including standing, climbing stairs, kneeling, squatting, driving, walking, sitting, and heavy lifting were not associated with increased risk of knee OA in men.

Table 3 shows ORs determined using conditional logistic regression analysis mutually adjusted for potential risk factors. Various risk factors were entered into the conditional logistic model, comprising: heaviest reported weight; previous knee injury; and physical work at the principal occupation in men. Heaviest reported weight in the past (OR 6.01, 95% CI 1.18–30.5, $P < 0.05$), past injury of the knee (OR 6.25, 95% CI 1.13–34.5, $P < 0.05$), and physical work at the principal occupation (OR 6.20, 95% CI 1.40–27.5, $P < 0.05$) represented independent factors associated with knee OA after controlling for other risk factors (Table 3).

Discussion

The results of the present case-control study indicate that heavy weight in the past and previous knee injury are associated with knee OA in men. Also in men, the proportion engaged in physical work (factory, construction, agriculture, or fishery work) was significantly higher among cases than controls. These risk factors for male knee OA are similar to those seen for female OA knees. Although we have already reported the results elsewhere,[10] we briefly compared results for men and women. Table 4 shows ORs in women determined using conditional logistic regression analysis mutually adjusted for potential risk factors. Various risk factors were entered into the conditional logistic model, comprising: heaviest reported weight in the past; previous knee injury; regular bicycle use; physical work in initial occupation; sedentary work in initial occupation; number of jobs; and total working period, summarizing all years of all jobs that subjects worked. Heaviest reported weight in the past, past injury of the knee, and total working period in women represented independent factors associated with knee OA after controlling for other risk factors. The results of the present case-control study indicate that heavy weight in the past and previous knee injury are associated with knee OA in both men and women.

Several limitations apply to the present study. Firstly, this investigation was based on a relatively small number of male cases and controls. Before the start of the research, we had calculated the sample size. We accumulated 155 pairs of cases and controls based on assumed values of a 0.05 level of significance, 80% statistical power, 2.0 risk ratio, and the 30% prevalence of cases. As a result, we succeeded in identifying 160 cases (40 men, 120 women) >45 years old

Table 5. Comparison of risk factors for hip and knee osteoarthritis (OA) in Britain and Japan (combined results for men and women)

	Risk factors	Britain	Japan
Hip OA	Obesity	Yes	No
	Past joint disturbance	Yes	No
	Occupational factors	Yes (lifting)	Yes (lifting)
Knee OA	Obesity	Yes	Yes
	Past joint disturbance	Yes	Yes
	Occupational factors	Yes (kneeling/squatting)	Yes (physical work, working period)

who fulfilled the entry criteria for the study. Of the eligible cases, 138 (86.3%; 37 men, 101 women) agreed to participate. However, the lack of gender balance for cases resulted in a small number of male subjects, which might reduce statistical power, and thus might not have detected other risk factors among lifestyle variables. This could be due to the use of identical case definitions for subject selection as the case-control hip OA and British studies. Cases were defined as those suffering knee pain and walking difficulties, who were first diagnosed by an orthopedic surgeon as displaying a tibiofemoral joint with a radiographic grade of ≥3 on the Kellgren and Lawrence scale. Our previous comparative study of OA in the lumbar spine indicated that OA in the general population tends to display lower prevalence and severity in Japan than in Britain.[14] In addition, the small number of male cases reflects gender differences in prevalence of knee OA in Japan. As a second limitation in the present study, the response rate for controls (52.8%) was lower than that for cases (92.0%). The present results may therefore be subject to some degree of overestimation.

Obesity has previously been shown to display strong associations with risk of knee OA,[2–8] and epidemiological studies performed in Japan have confirmed associations between obesity and knee OA.[15,16] In the present study, a history of heavy weight was shown to exert significant influences on risk of knee OA among men, resembling the results of women,[10] and consistent with previous studies. These findings indicate that the influence of heavy weight on knee OA is consistent across gender in both Japanese and Western populations.

The involvement of other joints is believed to play a role in increased risk of OA. In the British study paralleling the present study, presence of Heberden's node and previous knee injury were both strongly and independently associated with knee OA.[11,12] Although the present study did not seek information regarding the presence of Heberden's node, information was obtained about past history of the involvement of other joints and areas, as diagnosed by a medical doctor, indicating an independent association between previous knee injury and knee OA. In particular, site of knee OA was basically in accordance with the injured site among cases with previous knee injured (right side 91.7%, left side 100%). These findings were again consistent among men and women across Japanese and Western populations.

Mechanical stress represents another factor in the pathogenesis of OA at any joint site. In the present study, although occupational activities of standing, climbing stairs, kneeling, squatting, driving, walking, and heavy lifting were not associated with increased risk of knee OA in men, physical work at the principal occupation raised the risk of knee OA. Physical work represented by factory, construction, agricultural, or fishery work for long periods involved mechanical stress on the knee joints. The previous report utilized conditional logistic regression analysis without physical work, and identified sedentary work as a preventive factor in women.[10] These occupational activities influencing the risk of knee OA suggest that excess stress at the joint raises the risk, while reduced load on the joint decreases risk.

The present case-control study of knee OA paralleled our previous study of hip OA,[9] and was identical in format to some British studies.[17,18] Table 5 summarizes the results of studies using the same methods, indicating differences in risk factors between hip OA and knee OA, and between populations in Britain and Japan. Occupational factors clearly influence the development of both of hip and knee OA in Japan, as in Britain, although differences exist in specific activities exerting influence. Moreover, previous joint injury represented a risk factor for knee OA in Japan, as in the British studies. Conversely, obesity did not represent an independent risk factor for hip OA in Japan, but was a risk factor for both hip and knee OA in the British studies. This may be because local mechanical factors such as acetabular dysplasia might exert stronger influences on hip OA in Japan than other general mechanical factors such as adiposity. However, these results suggest that the pathogenesis of knee OA is similar in Japan and Western countries. Further studies of OA in other sites are required to characterize the risk profile in Japan.

Acknowledgments This research was supported by Grants-in-Aid for Scientific Research A11770200 from the Ministry of Education, Science, Sports and Culture in Japan, the Japan Society for the Promotion of Science, Research Society for Metabolic Bone Diseases, Japan, and the Arthritis Research Campaign, UK. We wish to acknowledge the generosity of surgeons and internists in Saiseikai Wakayama Hospital, Wakayama; Hori Hospital, Sennan; Nishioka Orthopaedic Hospital, Arita; Ryujin Clinic, Wakayama; Tamai Orthopaedic Hospital, Hannan; and Yamamoto Clinic, Shimotsu, Japan; and of Mrs. Sumiko Suzuri for help in locating participants for interviewing. The results of

this study were presented in 2001 at the British Society for Rheumatology XVIIIth Annual General Meeting.

References

1. Murray CJL, Lopez AD. The global burden of disease. Geneva: World Health Organization; 1997.
2. Anderson JJ, Felson DT. Factors associated with osteoarthritis of the knee and the first national health and nutrition examination survey (NHANES-I): evidence for an association with overweight, race and physical demands for work. Am J Epidemiol 1988;128: 179–89.
3. Felson DT. The epidemiology of knee osteoarthritis: results from the Framingham Osteoarthritis Study. Semin Arthritis Rheum 1990;20 Suppl 1:42–50.
4. Spector TD. The fat on the joint: osteoarthritis and obesity. J Rheumatol 1990;17:283–4.
5. Felson DT, Zhang Y, Anthony JM, Naimark A, Anderson JJ. Weight loss reduces the risk for symptomatic knee osteoarthritis in women. Ann Intern Med 1992;116:535–9.
6. Hochenburg MC, Lethbridge-Cejku M, Scott WW, Reichle R, Plato CC, Tobin JD. The association of body weight, body fatness and body fat distribution with osteoarthritis of the knee: data from the Baltimore longitudinal study of aging. J Rheumatol 1995;22: 488–93.
7. Hart DJ, Doyle DV, Spector TD. Incidence and risk factors for radiographic knee osteoarthritis in middle-aged women: the Chingford Study. Arthritis Rheum 1999;42:17–24.
8. Cooper C, Snow S, McAlindon RW, Kellingray S, Stuart B, Coggon D, et al. Risk factors for the incidence and progression of radiographic knee osteoarthritis. Arthritis Rheum 2000;43:995–1000.
9. Yoshimura N, Sasaki S, Iwasaki K, Danjoh S, Kinoshita H, Yasuda T, et al. Occupational lifting is associated with hip osteoarthritis: a Japanese case-control study. J Rheumatol 2000;27: 434–40.
10. Yoshimura N, Nishioka S, Kinoshita H, Hori N, Nishioka T, Ryujin M, et al. Risk factors for knee osteoarthritis in Japanese women: heavy weight, past joint injuries and occupational activities. J Rheumatol 2004;31:157–62.
11. Cooper C, McAlindon T, Coggon D, Egger P, Dieppe P. Occupational activity and osteoarthritis of the knee. Ann Rheum Dis 1994;53:90–3.
12. Coggon D, Croft P, Kellingray S, Barrett D, McLaren M, Cooper C. Occupational physical activities and osteoarthritis of the knee. Arthritis Rheum 2000;43:1443–9.
13. Kellgren JH, Lawrence JS. Radiological assessment of osteoarthritis. Ann Rheum Dis 1957;16:494–502.
14. Yoshimura N, Dennison E, Wilman C, Hashimoto T, Cooper C. Epidemiology of chronic disc degeneration and osteoarthritis of the lumbar spine in Britain and Japan: a comparative study. J Rheumatol 2000;27:429–33.
15. Tamaki M, Koga Y. Osteoarthritis of the knee joint: a field study (in Japanese). Nippon Seikeigeka Gakkai Zasshi (J Jpn Orthop Assoc) 1994;68:737–50.
16. Suematsu N, Onozawa T, Suzuki S, Takemitsu Y, Niinuma R. Epidemiologic study of osteoarthritis of the knee in agricultural and forestry workers (in Japanese). Seikei Saigai Geka (Orthop Surg Traumatol) 1986;29:343–6.
17. Cooper C, Inskip H, Croft P, Campbell L, Smith G, McLaren M, et al. Individual risk factors for hip osteoarthritis; obesity, hip injury, and physical activity. Am J Epidemiol 1998;147:516–22.
18. Coggon D, Kellingray S, Inskip H, Croft P, Campbell L, Cooper C. Osteoarthritis of the hip and occupational lifting. Am J Epidemiol 1998;147:523–8.

nature medicine

LETTERS

Carminerin contributes to chondrocyte calcification during endochondral ossification

Takashi Yamada[1], Hirotaka Kawano[1], Yu Koshizuka[1], Toru Fukuda[2], Kimihiro Yoshimura[2], Satoru Kamekura[1], Taku Saito[1], Toshiyuki Ikeda[1], Yosuke Kawasaki[1], Yoshiaki Azuma[3], Shiro Ikegawa[4], Kazuto Hoshi[1], Ung-il Chung[1], Kozo Nakamura[1], Shigeaki Kato[2] & Hiroshi Kawaguchi[1]

Endochondral ossification is an essential process not only for physiological skeletal development and growth, but also for pathological disorders. We recently identified a novel cartilage-specific molecule, carminerin (also known as cystatin 10 and encoded by *Cst10*), which is upregulated in synchrony with cartilage maturation and stimulates the later differentiation of cultured chondrocytes[1]. Although carminerin-deficient (*Cst10*$^{-/-}$) mice developed and grew normally, they had a microscopic decrease in the calcification of hypertrophic chondrocytes at the growth plate. When we created experimental models of pathological endochondral ossification, we observed suppression of chondrocyte calcification during formation of osteoarthritic osteophytes, age-related ectopic ossification and healing of bone fractures in *Cst10*$^{-/-}$ mice. Cultured *Cst10*$^{-/-}$ chondrocytes showed a reduction in calcification with activation of an SRY site in the promoter of the gene encoding nucleotide pyrophosphatase phosphodiesterase 1 (NPP1, encoded by *Enpp1*). Functional NPP1 is required for carminerin deficiency to suppress the pathological endochondral ossifications listed above. Carminerin is the first cartilage-specific protein that contributes to chondrocyte calcification during endochondral ossification under physiological and pathological conditions through the transcriptional inhibition of NPP1.

We generated *Cst10*$^{-/-}$ mice by homologous recombination in mouse embryonic stem cells using a targeting vector to replace exon 1 with the phosphoglycerate kinase-neomycin (PGKneo) cassette (**Fig. 1a**). Inbreeding of heterozygous *Cst10*$^{+/-}$ mice yielded *Cst10*$^{-/-}$ mice, as determined by Southern blot analysis, at the expected mendelian ratio (**Fig. 1b**). Neither *Cst10* transcripts nor carminerin protein was detected in the rib cartilage of *Cst10*$^{-/-}$ mice, confirming disruption of the *Cst10* gene (**Fig. 1c,d**). *Cst10*$^{-/-}$ mice developed and grew similarly to wild-type (*Cst10*$^{+/+}$) and *Cst10*$^{+/-}$ littermates without abnormalities of major organs (**Fig. 1e,f**).

Radiological analyses of femurs and tibiae in 8-week-old mice showed that *Cst10*$^{-/-}$ mice experienced decreases in trabecular bone volume mainly at the metaphysis, but not in cortical bone at the diaphysis, as compared to the wild-type littermates (**Fig. 2a,b** and **Supplementary Fig. 1** online). Histological examination of the proximal tibias indicated a decrease in trabecular bone volume beneath the growth plate of *Cst10*$^{-/-}$ mice (**Fig. 2c**). Although expression of carminerin was localized mainly in the wild-type hypertrophic chondrocytes, the columnar architecture, expression of type X collagen (Col X) and the entire width of the growth plate were comparable between wild-type and *Cst10*$^{-/-}$ mice, indicating that hypertrophic differentiation of chondrocytes was not affected by the carminerin deficiency (**Fig. 2c,d**). The width of the calcified layer and the number of calcified chondrocytes, as determined by von Kossa staining, however, were reduced (**Fig. 2c,d**). Bone volume in the *Cst10*$^{-/-}$ primary spongiosa just beneath the growth plate was significantly reduced ($P < 0.01$), with normal numbers of tartrate-resistant acid phosphatase (TRAP)-positive chondroclasts or osteoclasts, whereas the secondary spongiosa was not affected (**Fig. 2c,d** and **Supplementary Fig. 1**). In vertebral bodies that undergo less longitudinal growth by the thinner growth plate than femurs and tibiae, the histomorphometric parameters were comparable between the two genotypes in the growth plate and the primary and secondary spongiosa (**Supplementary Fig. 1**). These findings indicate that the decrease in trabecular bone adjacent to the growth plate of *Cst10*$^{-/-}$ long bones under physiological conditions resulted primarily from impairment of the calcification of hypertrophic chondrocytes, but not from the abnormality of cartilage resorption by chondroclasts or bone formation by osteoblasts.

We then examined the involvement of carminerin in pathological endochondral ossification by using experimental models involving wild-type and *Cst10*$^{-/-}$ littermates. First, we investigated the role of carminerin in the pathogenesis of osteoarthritis by inducing instability in the mouse knee joint[2]. The joint cartilage destruction was similarly visible at the posterior of the tibias (**Fig. 3a**) in both genotypes. The

[1]Department of Sensory & Motor System Medicine, Faculty of Medicine, University of Tokyo, Hongo 7-3-1, Bunkyo, Tokyo 113-8655, Japan. [2]Institute of Molecular and Cellular Biosciences, University of Tokyo, Yayoi 1-1-1, Bunkyo, Tokyo 113-0032, Japan. [3]Teijin Institute for Biomedical Research, Asahigaoka 4-3-2, Hino, Tokyo 191-8512, Japan. [4]Institute of Physical and Chemical Research (RIKEN), Shirokanedai, Minato, Tokyo 106-8639, Japan. Correspondence should be addressed to H.K. (kawaguchi-ort@h.u-tokyo.ac.jp).

Received 1 January; accepted 7 April; published online 7 May 2006; doi:10.1038/nm1409

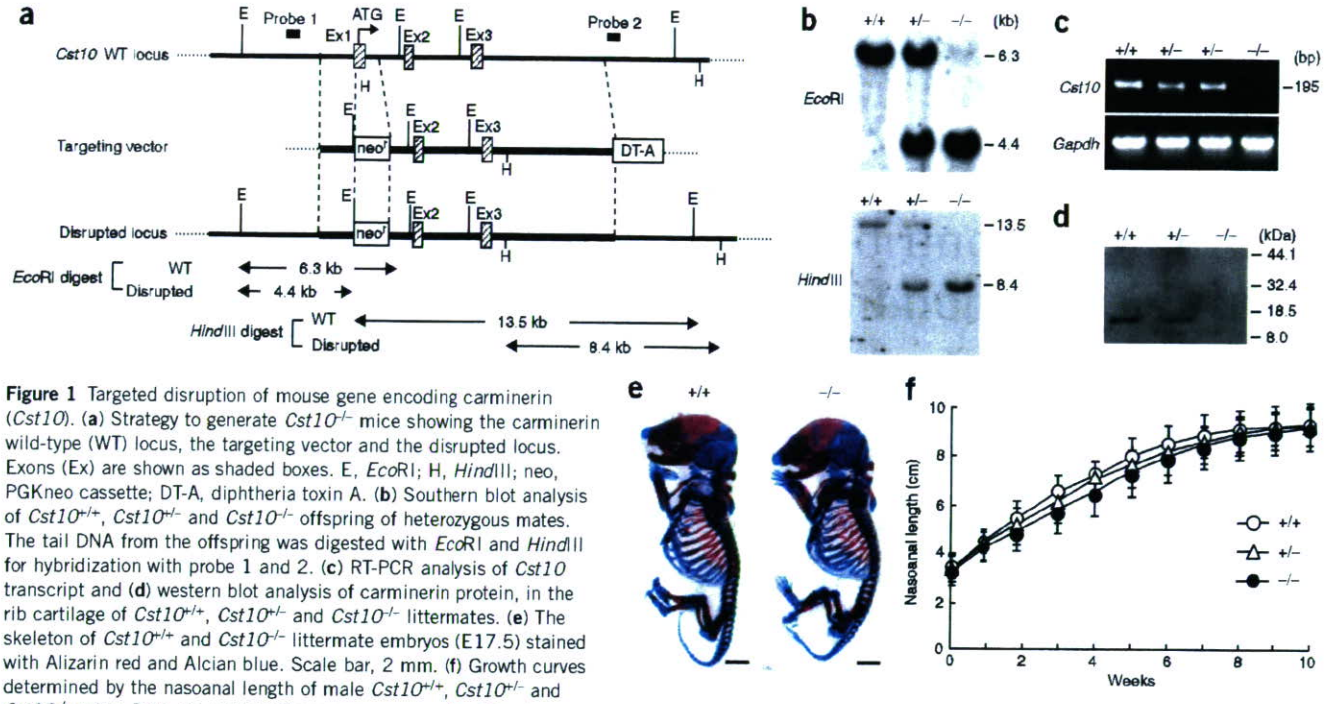

Figure 1 Targeted disruption of mouse gene encoding carminerin (*Cst10*). (**a**) Strategy to generate *Cst10*$^{-/-}$ mice showing the carminerin wild-type (WT) locus, the targeting vector and the disrupted locus. Exons (Ex) are shown as shaded boxes. E, *Eco*RI; H, *Hind*III; neo, PGKneo cassette; DT-A, diphtheria toxin A. (**b**) Southern blot analysis of *Cst10*$^{+/+}$, *Cst10*$^{+/-}$ and *Cst10*$^{-/-}$ offspring of heterozygous mates. The tail DNA from the offspring was digested with *Eco*RI and *Hind*III for hybridization with probe 1 and 2. (**c**) RT-PCR analysis of *Cst10* transcript and (**d**) western blot analysis of carminerin protein, in the rib cartilage of *Cst10*$^{+/+}$, *Cst10*$^{+/-}$ and *Cst10*$^{-/-}$ littermates. (**e**) The skeleton of *Cst10*$^{+/+}$ and *Cst10*$^{-/-}$ littermate embryos (E17.5) stained with Alizarin red and Alcian blue. Scale bar, 2 mm. (**f**) Growth curves determined by the nasoanal length of male *Cst10*$^{+/+}$, *Cst10*$^{+/-}$ and *Cst10*$^{-/-}$ mice. Data are expressed as mean ± s.e.m. for 15 mice per group. Females also showed similar skeletal development and growth in all genotypes.

carminerin expression was colocalized with Col X in the wild-type hypertrophic chondrocytes adjacent to the osteophyte (**Fig. 3b**). Although the hypertrophic differentiation of chondrocytes was not affected by the carminerin deficiency (**Fig. 3a**), osteophyte formation at the posterior of the tibias was significantly decreased (**Fig. 3a,c**). These findings confirmed by quantification by the Mankin grading score[3] and the osteophyte volume (**Fig. 3d**) indicate that carminerin produced in hypertrophic chondrocytes as a result of mechanical stress contributes to osteophyte formation through chondrocyte calcification, without affecting cartilage destruction or chondrocyte hypertrophy.

Similar findings were observed in ectopic ossification of the patellar ligament and the Achilles tendon with aging (**Supplementary Methods** online), which was significantly decreased by the carminerin deficiency ($P < 0.05$; **Supplementary Fig. 2** online). The colocalization of Col X and carminerin adjacent to the ectopic ossification indicates the involvement of carminerin-expressing hypertrophic chondrocytes in this disorder as well (**Supplementary Fig. 2**).

We further examined the involvement of carminerin in bone fracture healing at the midshaft of tibias[4,5]. *Cst10*$^{-/-}$ mice showed a bone gap upon X-ray 3 weeks after the fracture, with substantial formation of cartilaginous callus but impaired calcification, especially at the central area (**Fig. 4a**). Again, carminerin was expressed in the wild-type chondrocytes adjacent to the calcified callus. The time course of bone mineral content (BMC) showed that calcification in the central one-third portion, but not in the peripheral two-thirds portion, was significantly reduced during the endochondral ossification period (2–7 weeks after fracture) in the *Cst10*$^{-/-}$ callus, although bone union was eventually achieved from the *Cst10*$^{-/-}$ small callus through unaffected bone formation and remodeling thereafter (**Fig. 4b**). This model also indicates that the carminerin deficiency impaired endochondral ossification, but not intramembranous ossification or osteoblastic bone formation.

The effects of carminerin deficiency on endochondral ossification under the pathological conditions above were more obvious than those under physiological conditions, which showed only a microscopic change. The phenotype of the physiological *Cst10*$^{-/-}$ growth plate was milder than that seen in other disorders such as vitamin A deficiency, which causes not only impaired chondrocyte calcification but also insufficient resorption of unmineralized cartilage by chondroclasts, leading to a suppressed skeletal growth[6]. The difference may be caused by operation of compensatory mechanisms for endochondral ossification, including osteoblastic bone formation and remodeling unaffected by the carminerin deficiency, which are sufficient to compensate for the deficiency under physiological conditions, but not so under pathological conditions.

Carminerin was originally called cystatin 10 because its amino acid sequence contained similarity to the cystatin protein family; however, our examination has not detected legitimate cystatin activity, which inhibits cysteine proteinases (**Supplementary Table 1** and **Supplementary Methods** online). We therefore renamed this protein carminerin after 'cartilage mineralization'. To elucidate the actual mechanism of carminerin action on endochondral ossification, we compared *ex vivo* cultures of chondrocytes isolated from the growth plates of the wild-type and *Cst10*$^{-/-}$ tibias (**Supplementary Methods**). Although chondrocyte proliferation and differentiation were similar between the two genotypes, chondrocyte calcification was suppressed in the *Cst10*$^{-/-}$ culture (**Supplementary Fig. 3** online), indicating a cell-autonomous effect. In contrast, *ex vivo* cultures of primary osteoblasts obtained from wild-type and *Cst10*$^{-/-}$ calvariae confirmed that these cells do not express carminerin, so that there was no difference of bone formation by osteoblasts in this bone type (**Supplementary Fig. 3**).

As inorganic pyrophosphate (PPi) is known to be a crucial inhibitor of calcification[7], we compared the expression of a few molecules that

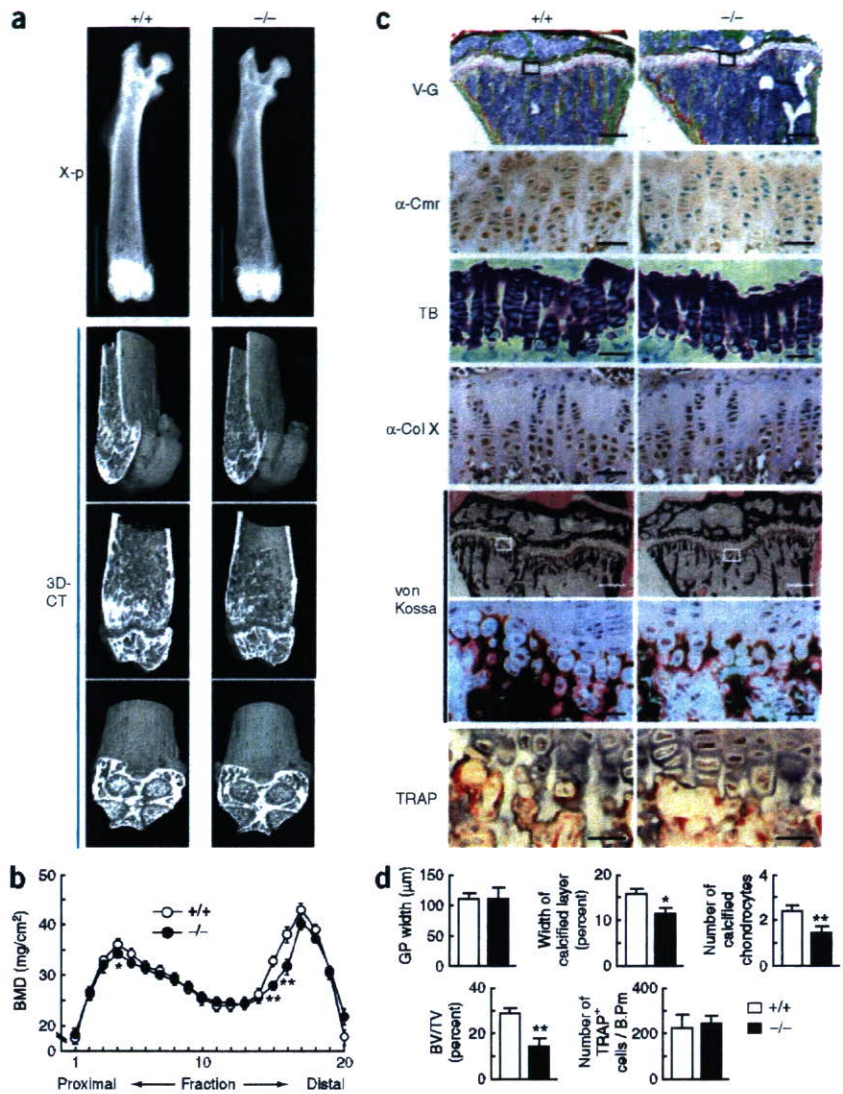

Figure 2 Radiological and histological findings of the long bones in wild-type (*Cst10*$^{+/+}$) and *Cst10*$^{-/-}$ littermates at 8 weeks of age under physiological conditions. (**a**) Plain X-ray of whole femurs, and three-dimensional computed tomography images of the distal part shown as green lines on the plain X-ray. (**b**) Bone mineral density (BMD) of the 20 equally divided fractions of femurs. (**c**) Histological findings of the proximal tibias. Villanueva-Goldner staining (V-G; scale bar, 200 μm). Inset boxes indicate the regions of the following three rows: immunostaining with an antibody to carminerin (α-Cmr; scale bar, 20 μm), toluidine blue staining (TB; scale bar, 20 μm), immunostaining with an antibody to Col X (α-Col X; scale bar, 20 μm). von Kossa staining (scale bars, 200 μm (top) and 20 μm (bottom)). Inset boxes indicate the regions of the bottom two rows: von Kossa staining and TRAP staining (scale bar, 20 μm). (**d**) Histomorphometric analyses of the growth plate and primary spongiosa just beneath it. The entire growth plate width (GP width) was measured on the TB sections, and the percent width of calcified layer to the entire growth plate and the number of calcified chondrocytes per column were measured on the von Kossa sections. Bone volume/tissue volume (BV/TV) and the number of TRAP^{+} cells in 100 mm of bone perimeter were measured in the primary spongiosa. Data are expressed as mean ± s.e.m. for 15 mice per group. $^{*}P < 0.05$, $^{**}P < 0.01$ compared to wild-type mice.

control the level of PPi in the cultured growth-plate chondrocytes, including: NPP1, which generates PPi from nucleoside triphosphates using nucleoside triphosphate pyrophosphohydrolase (NTPPPH) activity[8], tissue-nonspecific alkaline phosphatase (TNAP) which hydrolyzes PPi[9], and the multiple-pass transmembrane protein ANK, which mediates intracellular-to-extracellular channeling of PPi[10]. Among these proteins, the carminerin deficiency upregulated expression of only NPP1, and accordingly, increased NTPPPH activity (**Supplementary Fig. 3**). The reintroduction of carminerin into *Cst10*$^{-/-}$ chondrocytes (Ax-*Cmr*) restored the abnormalities in calcification, expression of NPP1 and NTPPPH activity to those similar to the wild-type culture (**Supplementary Fig. 3**). The promoter activity of an *Enpp1* promoter-luciferase construct (–964 *Enpp1* promoter-Luc) transfected into ATDC5 cells overexpressing carminerin (pCMV-*Cmr*/ATDC5) was lower than cells transfected with mock vector (pCMV/ATDC5; **Supplementary Fig. 3**). Deletion analysis of the *Enpp1* promoter region identified the core responsive element between the –360 and –324 regions, within which an SRY (sex-determining region Y) consensus sequence was predicted. Site-directed mutagenesis to eliminate the SRY site canceled the inhibition of *Enpp1* transcription by carminerin. Electrophoretic mobility shift assay confirmed specific binding of the SRY region by an oligonucleotide probe with nuclear extracts prepared from pCMV/ATDC5 and pCMV-*Cmr*/ATDC5 cells. Binding by the probe was weaker with the pCMV-*Cmr*/ATDC5 extracts than with the pCMV/ATDC5 extracts (**Supplementary Fig. 3**). As the binding was not detected using the synthetic carminerin protein instead of the nuclear extracts, carminerin itself was shown not to be the direct transcription factor for the SRY region. In contrast, nuclear extracts from the primary *Cst10*$^{-/-}$ growth plate chondrocytes showed stronger binding with the SRY site than those from the wild-type chondrocytes (**Supplementary Fig. 3**). Hence, the transcriptional inhibition of NPP1 expression by carminerin may result, at least partly, from the impaired binding of a transcription factor to the SRY site of the *Enpp1* promoter. Although Sox9, a potent regulator of chondrocyte differentiation[11,12], is the most probable transcription factor for this site, we did not observe a supershift of the DNA-protein complex when we added Sox9-specific antibody in the electrophoretic mobility shift assay (data not shown), indicating the involvement of other transcription factors in the regulation of the SRY site. In addition, in our efforts to identify the upstream regulator of NPP1, we did not find substantial regulation of expression or transcription of NPP1 by carminerin through the cytokines interleukin-1β (IL-1β), fibroblast growth factor-2 (FGF-2) or transforming growth factor-β (TGF-β), which previously have been reported to regulate NPP1 expression[13–15] (**Supplementary Fig. 4** online). Thus, further studies to elucidate a more detailed mechanism through which carminerin inhibits transcription of NPP1 will be necessary.

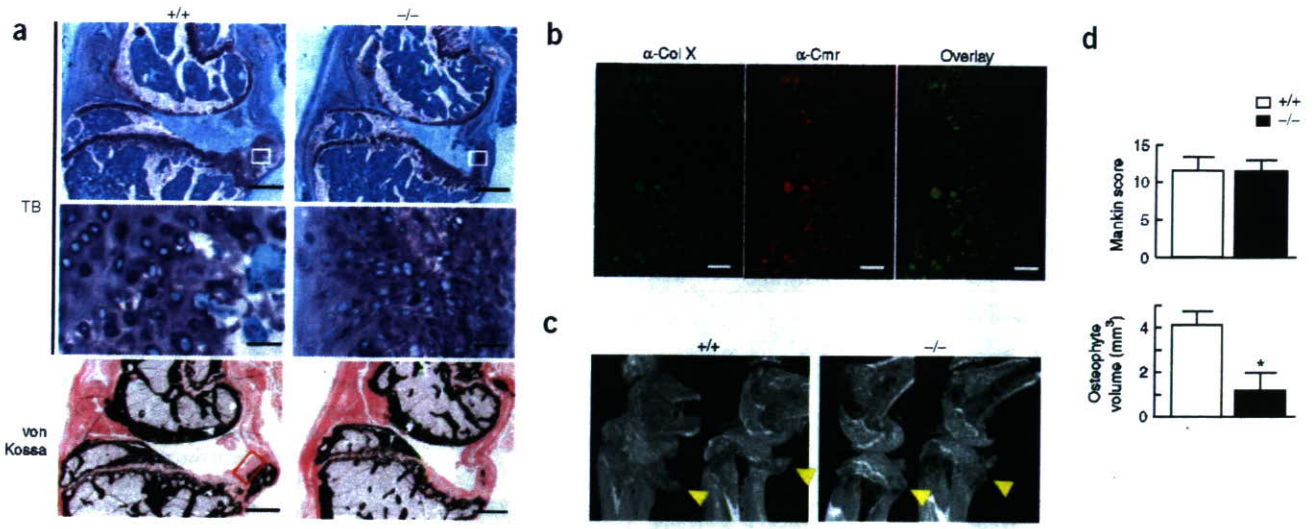

Figure 3 Histological and radiological findings of osteoarthritic joints in wild-type (*Cst10*$^{+/+}$) and *Cst10*$^{-/-}$ littermates. (**a**) Osteoarthritis was induced at the posterior tibias of the knee joint of 8-week-old mice by surgically imposing instability to the joint. Histological features; toluidine blue (TB; inset boxes in the top figures indicate regions shown in middle row; scale bars, 200 μm (top) and 20 μm (middle)) and von Kossa stainings (scale bar, 200 μm) of the sagittal sections of knee joints 10 weeks after surgery (left side of each photo is anterior side). (**b**) Immunostainings with an antibody to Col X (α-Col X, green), an antibody to carminerin (α-Cmr, red) and the overlay (yellow) analyzed by confocal microscopy in the region indicated in the inset of the image of von Kossa staining of wild-type knee in **a**. Scale bar, 20 μm. (**c**) Three-dimensional computed tomography images of the knee joints from the posterolateral projection. Arrowheads indicate osteophytes. (**d**) Quantification of the cartilage destruction and the osteophyte formation as determined by the Mankin grading score (top) and the osteophyte volume measured on the three-dimensional computed tomography images (bottom), respectively. Data are expressed as mean ± s.e.m. for ten mice per group. $^{*}P < 0.01$ compared to wild-type mice.

Finally, we carried out *in vitro* fertilization and embryo transfer from *Cst10*$^{-/-}$ mice and the *Enpp1*$^{-/-}$ mice, which lack expression of functional NPP1 (ref. 16), and generated four genotypes of mice: *Cst10*$^{+/+}$*Enpp1*$^{+/+}$, *Cst10*$^{-/-}$*Enpp1*$^{+/+}$, *Cst10*$^{+/+}$*Enpp1*$^{-/-}$ and *Cst10*$^{-/-}$*Enpp1*$^{-/-}$. When we used the experimental models, there was no difference in formation of osteoarthritic osteophytes, age-related ectopic ossification or high phosphate–induced auricular ossification between the NPP1-deficient mice (*Cst10*$^{+/+}$*Enpp1*$^{-/-}$) and the double-deficient mice (*Cst10*$^{-/-}$*Enpp1*$^{-/-}$), confirming that functional NPP1 is essential for suppression of the pathological endochondral ossification by the carminerin deficiency *in vivo* (**Supplementary Fig. 5** online).

Our previous *in vitro* study showed that overexpression of carminerin in ATDC5 cells accelerated not only calcification but also

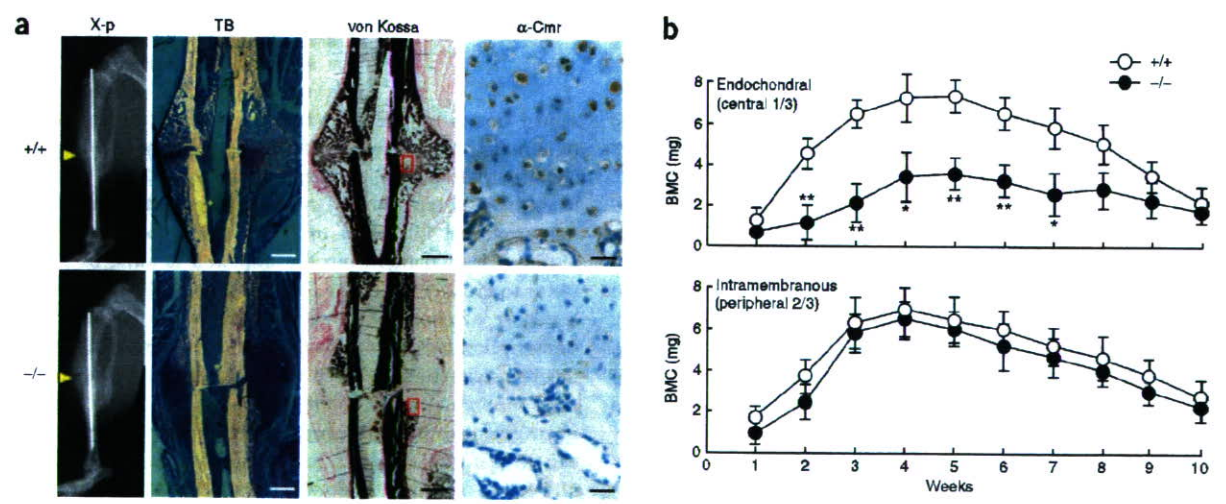

Figure 4 Radiological and histological findings of bone fracture healing in wild-type (*Cst10*$^{+/+}$) and *Cst10*$^{-/-}$ littermates. Fracture was produced by a transverse osteotomy that was stabilized with an intramedullary nail at the midshaft of tibias in 8-week-old mice. (**a**) Plain X-ray, toluidine blue (TB), von Kossa and a carminerin-specific antibody (α-Cmr) immunostainings 3 weeks after fracture. Insets in the image of von Kossa staining indicate regions of immunostaining. Scale bar, 20 μm for immunostaining, and 200 μm for the others. (**b**) Time course of bone mineral content (BMC) at the fracture callus for 10 weeks after fracture. BMC of the central one-third portion was measured as the endochondral ossification, and BMC of the peripheral two-thirds as the intramembranous ossification. Data are expressed as mean ± s.e.m. for six mice per time per group. $^{*}P < 0.05$, $^{**}P < 0.01$ compared to wild-type mice.